# Pleistocene-Holocene tectonic reconstruction of the Ballık travertine (Denizli Graben, SW Turkey): (de)formation of large travertine geobodies at intersecting grabens

*Non-peer reviewed preprint submitted to EarthArXiv*
*Paper in revision at Journal of Structural Geology*

Koen VAN NOTEN[1,2,4,*], Savaş TOPAL[3], M. Oruç BAYKARA[3], Mehmet ÖZKUL[3], Hannes CLAES[4,♦], Cihan ARATMAN[3,4] & Rudy SWENNEN[4,*]

[1] *Geological Survey of Belgium, Royal Belgian Institute of Natural Sciences, Jennerstraat 13, 1000 Brussels, Belgium*

[2] *Seismology-Gravimetry, Royal Observatory of Belgium, Ringlaan 3, 1180 Brussels, Belgium*

[3] *Department of Geological Engineering, Pamukkale University, 20070 Kınıklı Campus, Denizli, Turkey*

[4] *Geodynamics and Geofluids Research Group, Department of Earth and Environmental Sciences, Katholieke Universiteit Leuven, Celestijnenlaan 200E, 3001 Leuven, Belgium*

♦ *now at Clay and Interface Mineralogy, Energy & Mineral Resources, RWTH Aachen University, Bunsenstrasse 8, 52072 Aachen, Germany*

[*]Corresponding authors
koen.vannoten@seismology.be (K. Van Noten)
rudy.swennen@kuleuven.be (R. Swennen)

## Highlights:

- A new fault map of the entire eastern margin of the Denizli Basin is presented
- Pleistocene travertine deposition occurred along an already present graben morphology
- Dominant WNW-ESE normal faults reflect dominant NNE-SSW extension
- Ballik area acted as a transfer zone during transient NW-SE extension
- Complex fault networks at intersecting basins are ideal for creating fluid conduits

## Graphical Abstract: See Figure 14

# Abstract

The Ballık travertine geobody developed at the intersection of the NE margin of the Denizli Graben-Horst System (DGHS) and the neighbouring Baklan Graben. To investigate the formation of travertine geobodies and the development and reactivation of faults at intersecting grabens, travertine and faults were mapped in 35 travertine quarries that excavate the NE Denizli margin. The upper margin of the Ballık area comprises a subhorizontal travertine facies that is covered by siliciclastics that likely sourced from the uplifted margin flank north of the Ballık travertine. The travertine in the lower regions start with a similar subhorizontal facies but becomes more complex and evolves to travertine facies formed by a sloping topography with a domal architecture. Travertine precipitated from resurfaced carbonate-precipitating fluids, directly along the margin faults and the fracture network and diffuse through Neogene unconsolidated underlying sediments. From the Denizli basin floor to the uplifted graben shoulders, fault orientation is dominantly WNW-ESE oriented with major basin faults showing a left-stepping trend. Paleostress inversion of fault-slip data reveals that a long-lived, NNE-SSW extensional-transtension phase initiated the WNW-ESE oriented, graben-facing normal fault network in the Early Pleistocene. In the Middle Pleistocene, the Ballık area subsequently acted as a transfer zone between the neighbouring Baklan Basin and NE-SW oriented margin-bounding faults of the DGHS, during which the Ballık fault network was left-lateral strike-slip reactivated. In this period other large travertine geobodies precipitated along Baklan Graben margin faults. Earthquake focal mechanisms, underground spring travertine and fissure ridge orientation indicate a Late Pleistocene-to-current NNE-SSW extensional stress regime during which travertine precipitation moved to more central parts of the DGHS. Large travertine geobodies more likely form at graben intersections because they are susceptible to an enhanced fluid flow sourced from a complex fault-fracture network induced by recurrent stress permutations and fault reactivation during different tectonic regimes.


**Keywords**: travertine facies development; fault mapping; extension; transtension; strike-slip reactivation; paleostress analysis

# 1. Introduction

In situ reservoir characterization is most often based on the combination of seismic and core data. In particular for complex carbonate reservoirs, the sedimentological and tectonic features between core and seismic-scale are decisive for production. Outcrop analogue studies cover this scale-gap and their integration is thus indispensable in multidisciplinary complex carbonate reservoir characterization. Most carbonate reservoirs are naturally fractured from micro- to kilometre scale with fractures acting as highways for fluids in the reservoir. After cementation, however, they can also result in compartmentalisation. A proper understanding of the reservoir-scale fracturing behaviour is thus essential. Among continental carbonate reservoir analogues, travertines best represent the close interaction between sedimentation, crustal fluid circulation and, especially, neotectonic deformation in actively deforming tectonic regions (Hancock et al., 1999). The morphology or reservoir architecture of travertines is controlled by the paleo-topography. In addition, the depositional environment and facies classification in travertines and tufas are also based on paleo-topography, i.e. in the mound versus slope vs depression depositional environment (Guo and Riding, 1998). The paleo-topography itself is, however, strongly dependent on regional and local faulting, affecting spring water discharge and spring orifices that generated the necessary slopes to allow superficial fluid flow. Travertines are thus a prime example of neo-tectonic indicators. Hence, in order to deduce the paleotopography, possible tectonic tilting has to be taken into account. Sedimentological features can be used to deduce tectonic tilting. Conversely, tectonic tilting has to be deduced before interpretation of sedimentology, like paleo-flow direction, is possible. To properly interpret sedimentological analyses and reconstruct complex travertine build-ups, a detailed tectonic analysis thus always needs to accompany travertine sedimentology. Analysing the sedimentology and tectonic deformation of travertine occurrences allows to reveal the nearby presence of the fault-fracture network in the subsurface that provided the necessary fluid pathways, which may have interacted with basement rocks.

In actively deforming regions, faults control the occurrence, size and geometry of travertine deposits. Geometrically, travertines occur as isolated individual elongate fissure ridges and as (large) travertine geobodies deposited in flat pools or in slope-controlled travertine mounds. Whereas travertine growth along fissure ridges is considered to develop episodically (e.g. Mesci et al., 2008), with fluid expulsion and fissure propagation being impacted by earthquake activity (Brogi and Capezzuoli, 2014), large-scale travertine depositions can last for several thousands of years, being fed by an actively enhanced fault-fracture network. Structurally, travertines develop in the fractured hangingwall of normal faults (Altunel, 1994; Brogi, 2004; Brogi and Capezzuoli, 2009; Brogi et al., 2010; De Filippis and Billi, 2012; Brogi and Capezzuoli, 2014; Özkul et al., 2014), in shear zones (Faccenna, 1994; Faccenna et al., 2008), above fault tips or near their lateral end (Çakır, 1999; Kele et al., 2008), but the largest masses can develop in strain-releasing step-overs and along relay ramps

developed between margin-bounding faults (Altunel and Hancock, 1993b; Çakır, 1999; Hancock et al., 1999; Martínez-Díaz and Hernández-Enrile, 2001; Brogi et al., 2012; Temiz et al., 2013). Not only the travertine outline reveals the geometry of the underlying fault system, also systematic joints and faults cutting through the travertine can be used as stress indicators for the contemporary tectonic stress field that has affected the travertine area, either during or after deposition (Altunel, 1994; Kaymakçı, 2006). Joint propagation and morphology is hereby strongly influenced by the internal heterogeneity of the travertine (Hancock et al., 1999; Van Noten et al., 2013).

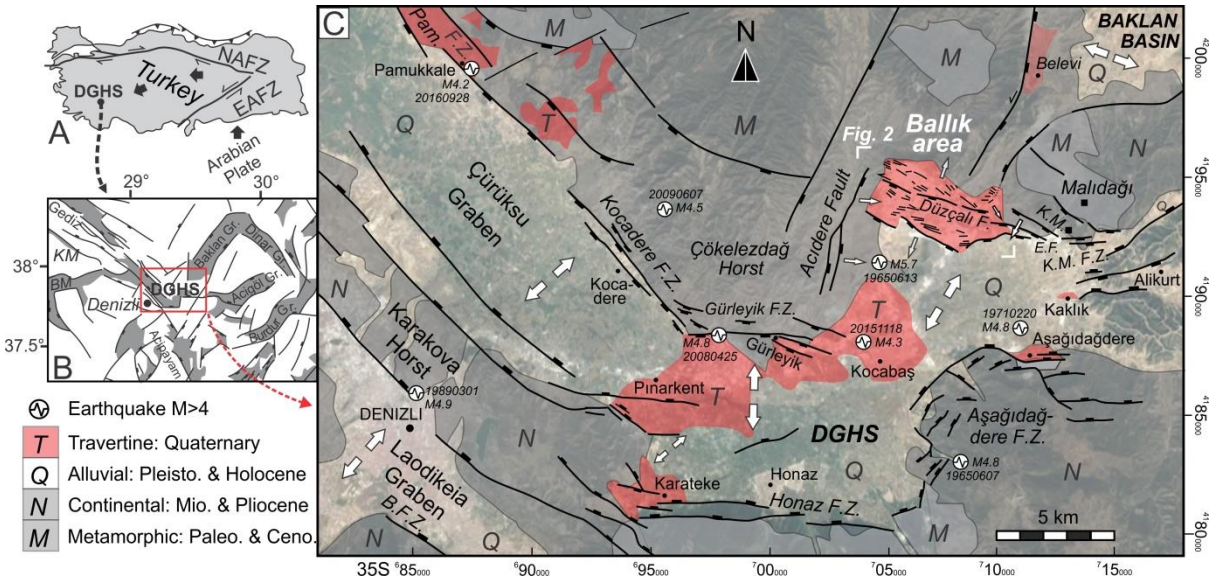


***Figure 1:*** *Geodynamic setting of the study area.* ***A)*** *Location of the Denizli Graben-Host System (DGHS) in Turkey. NAFZ: North Anatolian Fault Zone, EAFZ: East Anatolian Fault Zone.* ***B)*** *Overview of sedimentary basins in the West Anatolian Extensional Province. BM = Büyük Menderes Graben; KM: Küçük Menderes Graben.* ***C****) Fault map of the eastern DGHS. Faults are derived from geomorphology and from Koçyiğit (2005). The Ballık study area is located along the northern graben flank in the eastern part of the DGHS. Minor faults drawn in the Ballık area are discussed in this study. Different extension directions that have affected the DGHS are indicated. Location of the M5.7 13 June 1965 earthquake is taken from Westaway (1993), other earthquakes are taken from the USGS earthquake database. K.M.: Küyükmalı Mountain; E.F.: Elmalı fault. B.F.Z.: Babadağ Fault Zone. Map coordinates are in UTM (35S, WGS 84). Basemap © Google Earth™.*

Travertine occurrences in the Denizli Graben-Horst System (DGHS, Koçyiğit, 2005) in the West Anatolian Extensional Province (WAEP, southwest Turkey; Fig. 1A, B) are one of the best studied around the world. In the DGHS, the touristic UNESCO Pamukkale 'cotton castle' travertine, actively precipitating along the Pamukkale Fault Zone, is the most famous example. In the Pamukkale area, fault, fracture and fissure mapping and their relationship to seismic activity has been studied to link travertine deposition to the neotectonic context of the Denizli area (Altunel and Hancock, 1993b; a; 1996; Hancock et al., 1999; Özkul et al., 2002; Koçyiğit, 2005; Kaymakçı, 2006; De Filippis et al., 2012; De Filippis et al., 2013; Özkul et al., 2013; Brogi et al., 2014).

Recently, the large-scale Pleistocene Ballık travertine geobody (12.5 km²), which was deposited along the northeastern step-like faulted northern margin of the DGHS (Fig. 1C), received much attention as

reservoir analogue. In this region, travertines are both present along the uplifted margin flank and at the foot of the margin where they are exposed in a large, 2 km-long, ~70 m high, travertine domal structure (further referred to as the *Killik dome*) that developed on top of the ancient Neogene and Pleistocene basin fill. The fact that such a domal structure resembles to aggradational carbonate build-ups in Pre-Salt plays offshore Brazil (Buckley et al., 2013), in the Namibe Basin (Sharp et al., 2013) and offshore Angola (Saller et al., 2016) has increased the interest in the Ballık travertine as a potential reservoir analogue (Claes et al., 2015; De Boever et al., 2016). Along the northern and southern margin of the DGHS, margin-bounding faults are mostly characteristic of pure normal faulting or normal faulting with a small oblique-slip component (Altunel, 1994; Çakır, 1999; Koçyiğit, 2005; Kaymakçı, 2006). Several normal faults, (sub)parallel to the margin-bounding faults, cross-cut the domal structure in the Ballık area. Uncommon with respect to other margin-bounding faults or to focal mechanisms of recent earthquakes (Irmak, 2013), many purely strike-slip kinematic markers are present in the fault infill in the Killik dome (Van Noten et al. 2013). Strike-slip faulting has only rarely been observed in the DGHS. Altunel (1994) reported sinistral strike-slip faults offsetting man-made channels and structures at Hierapolis (Pamukkale) and a few minor WNW-striking strike-slip faults cutting through the fissure ridge at Koçabas. Van Noten et al. (2013) interpreted strike-slip faulting affecting the Killik dome to have occurred during a transient strike-slip stress field in the Pleistocene hereby reactivating the already existing normal faults. However, to date any link with a larger-scale regional tectonic model is still lacking and needs to be addressed.

Travertines are not only restricted to the Killik dome but dominate the entire northeastern upper graben flank of the DGHS. Altunel (1994) was the first to study these faults. Although these travertine masses constitute the largest part of the Ballık area and are intensively quarried, they hardly received any attention after Altunel's pioneering study. A detailed fault mapping and tectonic analysis of the entire NE Denizli graben flank was never performed. East and west of the Killik dome, travertine sequences consist mostly of subhorizontal bedded travertine that laterally extends for a few hundreds of meters. Also along the northern flank many lateral intercalations of fluvial conglomerate, sandstone, mudstone, paleosol horizons and erosional surfaces occur (Özkul et al., 2002).

With the aim of understanding the tectonic evolution of the entire northern graben flank of the Ballık area, a detailed structural analysis of the Ballık travertine is presented in this study. As travertines are heavily quarried in this area and evidences will be progressively removed in the near future, it is essential to document and report all structural features along this graben flank. This study therefore focuses on the orientation of major travertine structures and domes, on fault orientation and fault-slip kinematic data and on the fracture network. After a geometric analysis on the observed faults, a paleostress analysis is performed on the collected kinematic data. The resulting paleostress directions allow deducing if stress variations occurred during the deformation of the entire NE margin of the DGHS. The dip and orientation of the different travertine masses are only briefly described as a detailed facies analysis is beyond the scope of the study. This study provides an overview of tectonic

structures that overprinted the travertine deposits which serve as a tectonic framework for studies that further focus on facies analysis, geochemistry and sedimentology of the Ballık travertine from which the travertine geobody architecture can be reconstructed.

# 2. Tectonic framework

### *2.1 Turkey geodynamics*

The DGHS is a seismically active basin situated in the West Anatolian Extensional Province (WAEP) in SW Turkey (Fig. 1A). The WAEP developed from a complex interaction of large-scale plate tectonics in the Aegean and Anatolian areas. Due to northwards migration of the Arabian Plate, on the one hand, and the northwards roll-back subduction of the African Plate below the Anatolian Plate in the Aegean region, on the other hand, a westwards squeeze-out motion and an anticlockwise rotation affected the Anatolian plate (Fig. 1A) (McKenzie, 1970; Seyítoğlu and Scott, 1996). This movement was the main driver for the exhumation of the Menderes Massif in the Miocene (Westaway et al., 2005; Alçiçek et al., 2007; ten Veen et al., 2009; van Hinsbergen et al., 2010; Gessner et al., 2013). Subsequent tectonic relaxation resulted in the development of a pronounced extensional stress regime in West Anatolia as shown by the predominantly NE-SW to NW-SE trending grabens, cross-grabens and horst-graben structures developed from the Pliocene to the Quaternary (Westaway, 1993; Seyítoğlu and Scott, 1996; Bozkurt, 2001; ten Veen et al., 2009). Most of these margin-bounding seismogenic faults, including the Denizli margin faults, are still active and were responsible for a number of devastating earthquakes in historic and recent times (Taymaz and Price, 1992; Irmak and Taymaz, 2009; Irmak, 2013). The development and destruction of numerous ancient cities in the Denizli area was affected significantly by destructive earthquakes (estimated > M6) (Altunel, 2000; Piccardi, 2007). Continuous earthquake activity along the margin faults has affected the Pliocene to recent deposits near the margin as well as the poorly-lithified Quaternary sediments in the basin creating typical earthquake-related soft-sediment deformation structures (Topal and Özkul, 2014).

### *2.2 The Denizli Graben-Horst System*

The DGHS is surrounded by the E-W trending Gediz, Küçük Menderes and Büyük Menderes Grabens in the east, the NW-SE Acıpayam Graben in the south and NE-SW Baklan, Acigöl and Burdur Grabens developed on the Dinar fault in the northeast (Westaway, 1990; 1993; Price and Scott, 1994; Koçyiğit, 2005; Kaymakçı, 2006) (Fig. 1B). High-angle normal faults, expressed as steep topographic scarps, delimit these basins. Many of these conjugate graben systems are consistent with a NE-SW, NW-SE and N-S multidirectional extension (Bozkurt and Sözbilir, 2006; Gürbüz et al., 2012). The horst-graben morphology of the DGHS formed during alternating seismic periods of subsidence and tectonic uplift (Westaway et al., 2005). A full description of the successive lithologies from the

Miocene to recent Quaternary alluvial plain basin and travertine deposits can be found in Alçiçek et al. (2007) and Claes et al. (2015).

The NW-SE oriented western and central part of the DGHS can be separated into two Quaternary subgrabens, namely the Çürüksu and Laodikeia Grabens, separated by the uplifted Karakova Horst (Kaymakçı, 2006; Topal and Özkul, 2014). The Çürüksu subbasin forms a c. 50 km long basin that is bordered by the Pamukkale normal fault zone in the northeast (Fig. 1B). Along this fault zone several travertine deposits, among which the active UNESCO Pamukkale travertines, are precipitated in kilometer-wide, left-lateral step-over zones that are developed at the end or between different segments of NW-SE-trending normal margin faults (Altunel and Hancock, 1993b; Çakır, 1999; Hancock et al., 1999). Along the northern margin, travertine occurrences are present as complex travertine mounds (Altunel and Hancock, 1993a, b; Kele et al., 2011; Özkul et al., 2013) and as small individual fissure ridges which developed above different branches or step-overs of the NW-oriented margin faults (Altunel and Karabacak, 2005; De Filippis et al., 2012, 2013; Özkul et al., 2013; Yalçiner, 2013; Brogi et al., 2014).

The Ballık study area is situated at the southeastern end of the DGHS where the basin morphology changes from NW-SE to locally E-W, forming the lateral extend of the Acigöl Graben in the east. This part of the DGHS has a pronounced staircase geometry. The southern border is delimited by the E-W graben-facing, step-like Honaz fault zone that is separated from the Babadağ fault zone by the NW-oriented transfer zone at Karateke (Fig. 1C). The Honaz fault zone is dominated by normal to oblique-slip faults along which slickenlines all point towards the center of the basin, indicative of differential extension rate (Topal, 2012; Özkaymak, 2015). The Aşağıdağdere fault zone is situated at the most southeastern edge of the DGHS and consists of several short, closely-spaced fault segments that are dominated by oblique-slip normal faults (Koçyiğit, 2005). Along the northern margin, the NW-trending Kocadere fault zone is considered to be the prolongation of the Pamukkale fault zone (Fig. 1C). The short E-W to WNW-ESE normal faults NE of Pınarkent belong to the Gürleyik fault zone and mark the transition from the NW-SE trending to the E-W trending orientation part of the DGHS. It is unknown if these smaller faults continue and maintain their trend towards the WNW-ESE oriented travertine fissure ridge at Kocabaş (Hancock et al., 1999; Özkul et al., 2002; Altunel and Karabacak, 2005; De Filippis et al., 2012).

Between Kocabaş and the Ballık area, the DGHS has a NW-SE to ENE-WSW orientation (Fig. 2). In the west, this subbasin is bounded by the N-S Acıdere fault which separates the flat Denizli basin floor in the east from the uplifted Çökelezdağ Horst in the west. The Ballık area is situated along the northern margin and is characterised by several closely-spaced, mainly WNW-ESE faults that are mapped and addressed in detail in this study. NE of the study area, the eastern margin fault of the Baklan Graben intersects with the DGHS.

### *2.3 Travertine of the Ballık area*

The mountain range front at Ballık, situated 25 km ENE from the city of Denizli, can clearly be recognised on ASTER satellite images, SRTM DEM and Google Earth™ images (see kml in supplementary material). The Ballık area forms a steep hill which starts at a basin floor altitude of c. 500 m asl. and reaches a maximum height of 877 m in the west at the Taşkestik Tepe (Fig. 2), i.e. 377 m above the current Denizli basin floor resulting from systematic Quaternary uplift. From top to bottom along the graben flank, travertine deposits are exposed along stepped, SW-, graben-facing slopes. 35 quarries that have excavated this large area are addressed in this study. The Ballık travertine, also referred to as the eroded-sheet travertines (sensu Altunel, 1994) or Kocabaş travertine geobody (Hancock et al., 1999; Khatib et al., 2014; Lebatard et al., 2014), is by far the largest travertine site in southwest Turkey (12.5 $km^2$) with travertine thickness up to at least 120 m (Özkul et al., 2013). The Ballık travertine has been widely used around the world since ancient times as a construction stone due to its good mechanical resistance and durability properties (Çobanoğlu and Çelik, 2012; Çelik et al., 2014).

Based on the morphology of the northern graben flank, a northern upper margin area can be separated from the Killik dome. The quarries excavating the Killik dome, i.e. the Faber, Ece, Tetik, Çakmak, İlik, Alimoğlu and Best abandoned (abandoned is further noted as *Ab.*) quarries (see Fig. 2 and kml in Suppl. Mat. for location of the quarries), were already the subject of several sedimentological and geochemical (Özkul et al., 2013; Khatib et al., 2014; Claes et al., 2015; El Desouky et al., 2015; Claes et al., 2017b; De Boever et al., 2017), geomechanical (Çobanoğlu and Çelik, 2012; Çelik et al., 2014), dating (Lebatard et al., 2014), petrophysical (Soete et al., 2015; De Boever et al., 2016) and structural (Van Noten et al., 2013) studies.

The Killik dome is characterised by horizontally bedded travertine at its base that gradually changes upwards into complex, slope travertines that are dominated by biohermal reed, cascade and waterfall travertine facies (Özkul et al., 2013; Claes et al., 2015; De Boever et al., 2017). Travertines precipitated from resurfaced meteoric waters that infiltrated along the margin that was already affected by a fault-fracture network. Fluids emerged as heated geothermal waters along the margin faults after having migrated through and interacted with the Lycian basement rocks (Claes et al., 2015; El Desouky et al., 2015). In a later stage, secondary fluid circulation was established with meteoric water interacting at depth and precipitated as calcite veins grown in faults and in the solution-enlarged fracture network cutting the travertine (Van Noten et al., 2013; El Desouky et al., 2015).

## 3. Methodology

The northern graben flank was investigated during an extensive field campaign in 2014 and several revisits in 2015 and 2016. Our study focuses on brittle structures such as joints (barren fractures

without any slip), open fissures (no displacement and infill), faults and fault kinematic indicators including slickensides, slickenlines and displaced travertine lamination and paleosols. The orientation of planar structures is reported as dip direction/dip (*e.g.* P270/80 for a fault plane dipping steeply to the west) whereas linear features are reported as trend/plunge (*e.g.* L090/85 for a slickenline plunging steeply to the east). Fault/fracture orientation analysis is performed with the program Stereo 32 (Röller and Trepmann, 2003). Kinematic data of faults and fractures collected in the quarries are visualised in lower hemisphere, equal-area projection stereoplots in the figures and raw fault/fracture measurements are available per quarry in Suppl. Mat. S2.

Quarries in the Ballık area were systematically investigated for the presence of faults. The 2013 Google Earth™ satellite image was used as basemap in all figures as this compares most closely with actual quarry situation during the main 2014 fieldwork. Due to continuously moving excavation fronts of the active quarries, quarry walls on current Google Earth images may no longer be in the same position as indicated in the figures in this study. Accurately-taken GPS points of individual observations (with a Trimble Geoexplorer GPS) were used to analyse if the position of the analysed excavation fronts was different than that on the Google Earth satellite image. GPS points are indicated on the fault map figures as small white dots to illustrate where faults were observed. Between travertine quarries, these individual fault observations were strategically linked to map out along-strike fault continuity.

With the geometrical fault dataset, a paleostress analysis is performed on the collected data. Principal stress directions can be derived from inversion of fault slip kinematic data. Most paleostress inversion techniques assume the Wallace-Bott hypothesis (Wallace, 1951; Bott, 1959), which state that fault slip should occur parallel to the resolved shear stress on a pre-existing or newly formed fault plane. Inversion of fault-slip data involves the concept of deriving a best-fitting tensor that can explain the direction of slip of the observed faults. The paleostress tensor and the principal stress directions responsible for the (re)activation of the observed faults were derived from the Right Dihedral Method (Angelier and Mechler, 1977) optimised in the Win-Tensor Program (version 5.0.2). This program has the advantage that based on their kinematic features, different phases of faulting can be separated semi-automatically. The different applied steps and quality control of paleostress inversion are described in Delvaux and Sperner (2003) and in Kipata et al. (2013).

## 4. Tectonic analysis of the Ballık area

To facilitate the description of the structural features, we separate the study area in five different domains. This separation is made according to the observed fault kinematics characterising each domain (Fig. 2). The focus is on 1) large-scale faults cutting through the Ballık travertine; 2) the NE extensional domain; 3) the NW extensional domain; 4) the eastern and 5) western extensional and strike-slip reactivated domain; 6) the strike-reactivated domain in the footwall of Düzçalı fault; and 7)

the Killik domal area and Southern Ballık area. The fault-fracture deformation for each quarry is shortly described in this section. All domains, fault data, quarry locations, fault observations and dip of the studied travertine masses are also presented in a Google Earth™ kmz file provided in Supplementary Material (S1). Raw fault-fracture orientations are provided for reproducibility in S2.

### *4.1 Large-scale faults: The Elmalı, Düzçalı, Killik and Acıdere faults*

Several kilometre-scale faults cross-cut the Ballık area and can be deduced from the morphology of the mountain range-front. In the east of the area, the WNW-trending Küçükmalıdağ fault zone delimits the northeastern incipient margin of the DGHS. This two- to three kilometre wide and 10 km long fault zone developed at the base of the Küçükmalı and Malıdağ mountains and consists of three fault sets: i.e. the Düzçalı, the Küçükmalıdağ and Elmalı faults along which Jurassic-Cretaceous dolomitic limestone, Upper Oligocene conglomerate, Middle Miocene clastics and Quaternary travertine and alluvial-plain sediments are tectonically juxtaposed (Koçyiğit, 2005). The **Küçükmalıdağ** and **Elmalı faults** are present east of the travertine excavation area. At the base of the Küçükmalı mountain (east of the cement factory, see eastern part of Fig. 2), eroded Neogene terraces dip towards the mountain flank due to activity along the listric Elmalı fault. Although Koçyiğit (2005) reported that the lateral end of the Elmalı fault should also be present just north of the Denizli Cement Factory (Fig. 2), no significant geomorphological or tectonic fault traces that support this observation were found.

The **Düzçalı fault** consists of four SW-, graben-facing, lerft-stepping fault segments of ~1 km in length. These segments can be traced in the field as the footwall is always a steep hill that consists of travertine, whereas the hangingwall has a gentle topographic slope along which fan-apron cover sediments are deposited. According to Koçyiğit (2005) and Altunel (1994), normal displacements along the Düzçalı fault reach up to c. 200 m. Fault surfaces dominantly contain steeply-dipping slickensides with only a minor dextral strike-slip component. However, in a small abandoned quarry at the western end of the Düzçalı fault subhorizontal strike-slip slickenlines (L280/16) overprint older steeply-plunging dip-slip slickenlines (L285/74) on a fault scarp (Fig. 3A) and indicate fault reactivation. This observation explains why both normal and strike-slip slickenlines were reported in the Düzçalı fault orientation analysis of Koçyiğit (2005).

Travertine is nowhere further excavated than at the southern border of the Killik dome where it is bordered by the Killik fault. The **Killik fault** has a dominant WNW-ESE orientation (Fig. 2). In the east, its orientation changes from WNW-trending to NE- and ENE-trending as a left-lateral step-over towards the Elmalı fault. In the west, south of the Tetik and Özçınar quarries (Fig. 2), fault orientation remains NW-SE but its position is translated by 500 m southwards as can be seen by the change in morphology of the mountain range-front. The Killik and Elmalı faults are considered to be active as indicated by range-front hydrothermal springs and few small-magnitude earthquakes, such as for instance the 3 November 1993 $M_L$ 3.6 and 12 April 1994 $M_L$ 3.3 earthquakes.

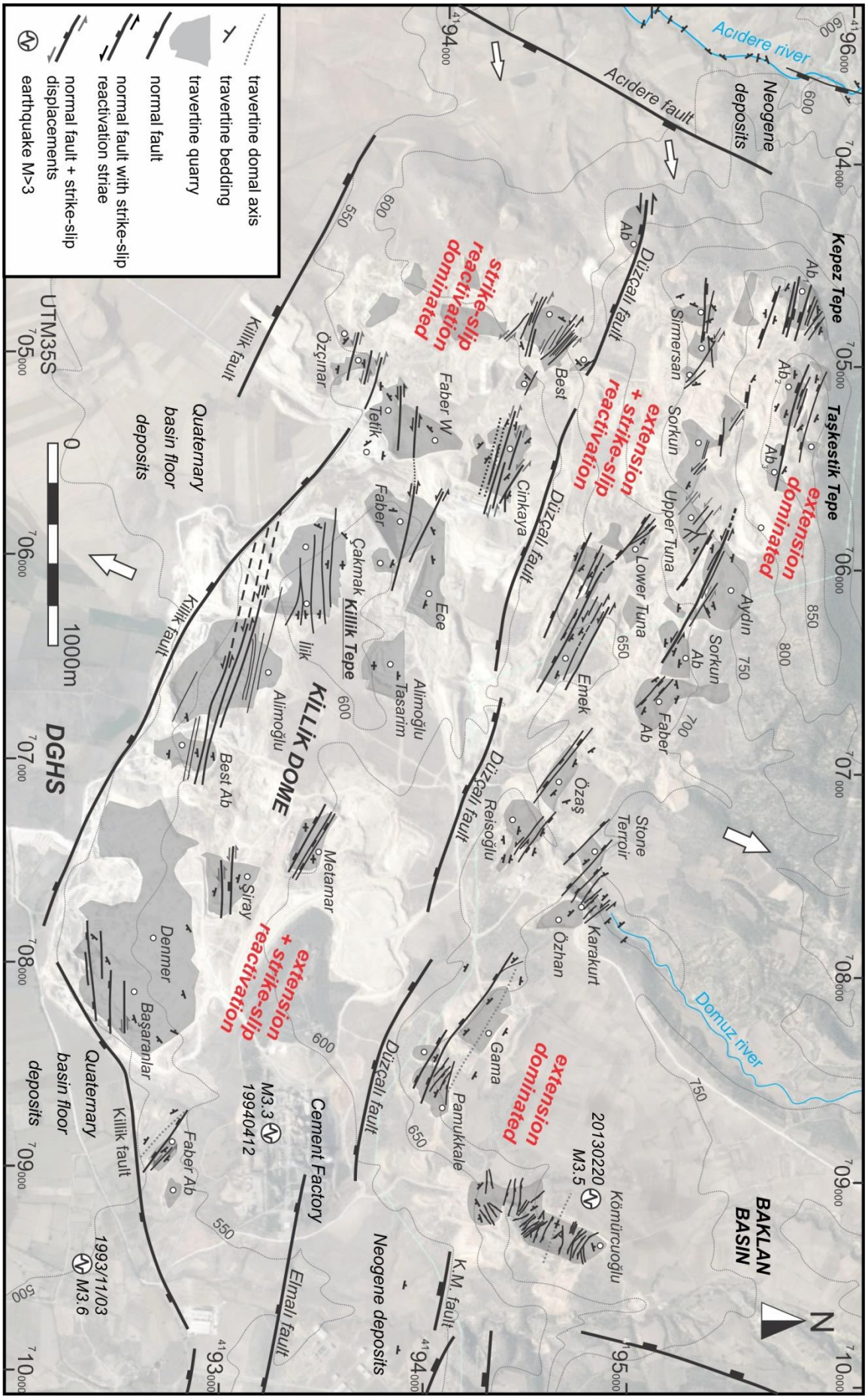
travertine domal axis
travertine bedding
travertine quarry
normal fault
normal fault with strike-slip reactivation striae
normal fault + strike-slip displacements
earthquake M>3
Acıdere river
Acıdere fault
Neogene deposits
Kepez Tepe
Taşkestik Tepe
Düzçalı fault
Killik fault
Simersan
Sorkun
Upper Tuna
Lower Tuna
Best
Cinkaya
Faber W
Tetik
Özçınar
Faber
Çakmak
Killik Tepe
Ece
Alimoğlu
Tasarim
Killik DOME
Best Ab
Metamar
Şiray
Denmer
Başaranlar
Quaternary basin floor deposits
DGHS
strike-slip reactivation dominated
extension + strike-slip reactivation
extension dominated
Aydın
Emek
Özaş
Reisoğlu
Stone Terroir
Karakurt
Özhan
Gama
Pamukkale
Domuz river
Kömürcuoğlu
20130220 M3.5
BAKLAN BASIN
Cement Factory
M3.3 19940412
1993/11/03 M3.6
K.M. fault
Elmalı fault
Neogene deposits
Faber Ab
UTM35S
0
1000m
N

347

***Figure 2:*** *Ballık fault map. Grey areas outline the different quarries and refer to the excavation fronts in 2013 (basemap © Google Earth). Coordinates are in UTM 35S. Eye altitude of satellite image is 5.07 km. The Düzçalı fault segments and the large normal faults bordering the travertine excavation area are derived from geomorphology and after Koçyiğit (2005). Topographic isohypses are taken from the 1:25 000 Denizli M22-B1-B4 topographic maps (1989) illustrating the original topography before excavation of the northern flank. White dots = quarries; Ab = Abandoned quarry; K.M. (F.Z.) = Küçükmalıdağ (Fault Zone); black strike-slip arrows = observed sinistral displacement; grey strike-slip arrows = inferred sinistral displacement.*

West of the Ballık area, the DGHS is bordered by the N-S oriented, steeply E-dipping Acıdere normal fault (Figs. 1 and 2). The Acıdere fault is geomorphologically visible because Quaternary sediments in the hangingwall form the flat basin floor of the DGHS, whereas the hills and older Neogene deposits in the footwall are strongly eroded due to the uplift of the Çökelezdağ Horst (Figs. 1 and 2). The footwall of the Acıdere fault is eroded by the Acıdere river (Fig. 3B). In the Acıdere valley alternating Oligocene sandstone and mudstone beds are exposed of which bedding alternates between NW- and W-dipping and is gently folded (see bedding in NW corner of Fig. 2). The fact that these Oligocene beds tilt to the west is related to backtilting of the Çökelezdağ Horst. Few N-S-trending, E-facing normal faults (Fig. 3C), i.e. parallel to the Acıdere fault, affect these sediments and demonstrate the N-S faulted nature of this horst structure.

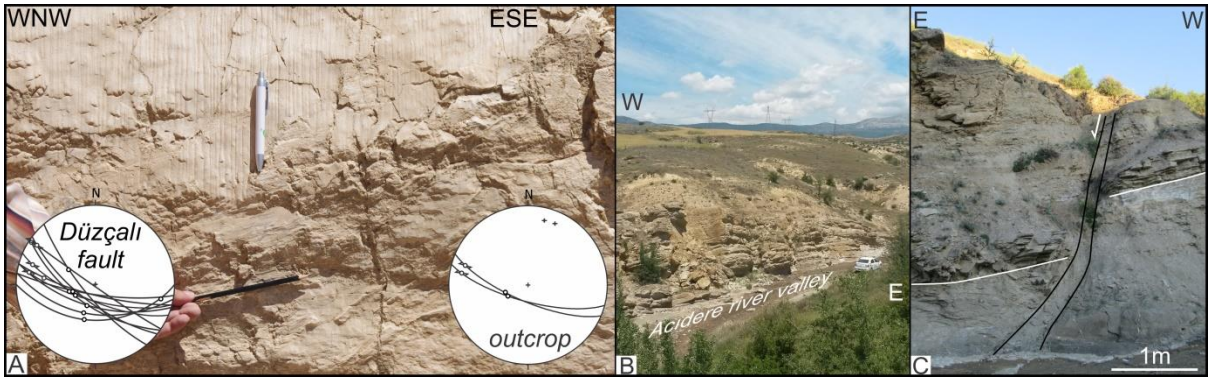


***Figure 3: A****) Fault scarp observed at the western tip of the Düzçalı fault in an abandoned quarry in the W Ballık area. Subhorizontal strike-slip slickenlines (L280/16) overprint steeply-plunging (L285/74) slickenlines. The right stereoplot displays fault and slickenline orientation in this outcrop. The left stereoplot illustrates all observations (including also data from Koçyiğit, 2005) of the Düzçalı fault in the Ballık area.* ***B****) W-dipping tilted Oligocene deposits in the Acıdere valley in the footwall of the Acıdere fault, Çökelezdağ Horst.* ***C****) N-S trending, E-facing normal fault affecting Oligocene sandstone and mudstone in the Acıdere valley.*

### *4.2 NE extensional domain: Kömürcüoğlu, Pamukkale & Gama quarries*

In the northeasternmost part of the Ballık area, the **Kömürcüoğlu** travertine is excavated (Figs. 2 and 4). Based on bedding orientation of travertine and the abundant presence of thin paleosols and intercalating conglomeratic layers, a WNW-ESE-oriented mound travertine structure is recognised. In the northern part of the quarry, travertine dips gently (< 10°) to the NNE. In the central part, the travertine is sub-horizontal while in the southern part of the quarry, a travertine lobe with a cascade- and waterfall facies (sensu Claes et al. 2015) dips gently to steeply (> 30°) to the SSW (Fig. 4B-B'). The top of the mound structure is covered by clastic sediments including conglomerates (Fig. 5F),

sandstone and marls. These sediments thicken from the NW to the SE suggesting a WNW-oriented dip of the top of the mound travertine structure (Fig. 4A-A'). In the southern part of the quarry, a 10 m-thick clastic layer of alternating layers of marls and sandstone laterally interfingers with the SSW-dipping end of the travertine structure (Fig. 5A). These layers are covered by subhorizontal travertine.

The majority of normal faults crossing the Kömürcüoğlu travertine have a NW-SE orientation. A minor amount is E-W oriented. In the southern part of the quarry faults are vertical to mostly steeply (up to 50°) north-dipping and have a northward normal displacement (Fig. 5B, 5C). In the northern part, all faults are subvertical to steeply south-dipping and have a decimetre- to metre-scale southward normal displacement (Fig. 5F). The location where faults change from N- to S-dipping lies close to the center of the travertine mound structure. Slickenlines on the fault walls are always dip-slip, only slightly deviating from verticality (Fig. 5D). Along strike, faults bifurcate into different fault branches and can have an S-shaped morphology.

At the contact between travertine and marl-dominated units, fault orientation refracts due to the ductile behaviour of the marly unit (Fig. 5A). This is the case with the normal faults that cross the interfingering marls (Fig. 4B-B'). Faults/fractures crossing the competent conglomeratic cover layers are very irregular along strike. Due to this irregularity, faults in cover sediments along the eastern quarry flank cannot be connected to the western part. As faults' orientation is irregular, they do not represent the regional extension. Hence, faults in cover sediments are illustrated separately in the orientation analysis in Figure 4 and will not be used for paleostress inversion.

Each fault has its own complex formation history. Opposite fault walls are often symmetrical (Fig. 5C) and are typically characterized by multiple succeeding phases of faulting, fault-parallel fluid flow, dissolution, brecciation and developments of striations by mechanical friction (Fig. 5D, E). Each of these different phases can later be cemented due to secondary fluid circulation. The faults are filled by brown oxidised mud, travertine clasts, debris and organic-rich material. The muddy and chaotic infill is indicative of the open nature of the faults during extension, enlarged by dissolution of the fault walls. Slickenlines are not always visible on the fault plane as secondary fluid flow has often overgrown these kinematic markers.

In a small quarry south of Kömürcüoğlu (S. quarry in Fig. 4), the edge of the travertine dome is excavated. Compared to the NW-SE-trending faults in the Kömürcüoğlu quarry, here, faults have a different NE-SW orientation. The displacement of these faults is, however, still northwards. In this quarry, metre-scale caves emplaced in biohermal reed facies are present (Fig. 5G). These caves are often covered by millimetre- to centimetre-thick alternating brown, white and beige banded secondary wall cements that can be seen around the entire cave. At the top of the cave hanging, pillar-shaped phyto plants are coated by cements giving rise to stalactite-like appearances hanging from the cave ceiling.

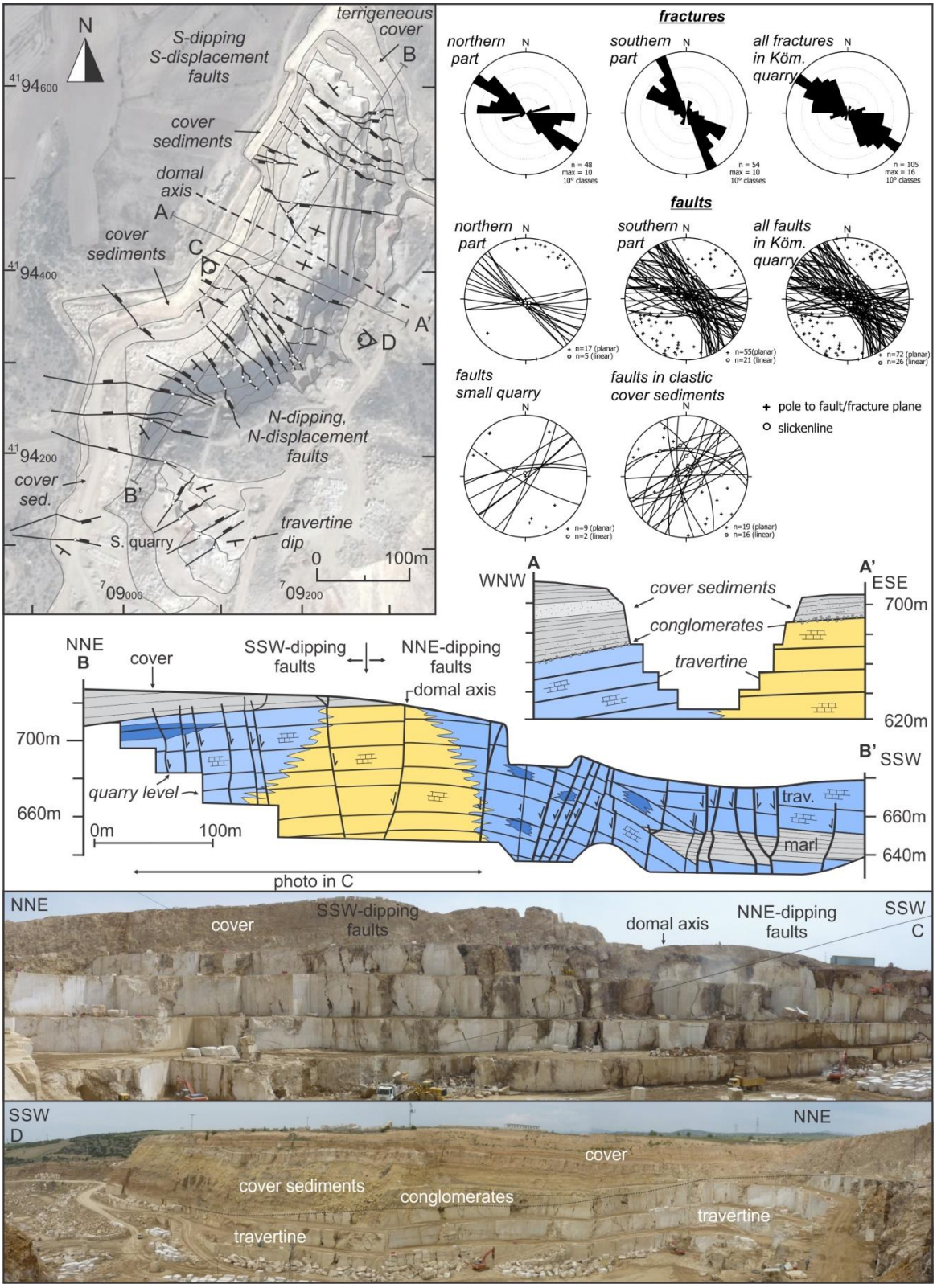


***Figure 4:*** *Fault map (basemap © Google Earth) and fault/fracture kinematic analysis (stereoplots) of the Kömürcuoğlu quarry (NE Ballık area). Note the different orientation of the faults in the small quarry in the south (S. quarry). The combined sedimentological and structural model shows that central sub-horizontal travertines (yellow) laterally continue into sloping cascade (blue) and waterfall facies (dark blue). The northern part is cut by upright to steeply S-dipping fractures and normal faults, with a southwards displacement, whereas the southern part is cut by north-dipping faults with northwards displacement. NW-dipping marly, conglomerate and sandstone (**A-A'**) cover the travertine dome. Marly deposits interfinger with the travertine structure (southern part of **B-B'**).*

Joints have similar orientations than the faults. In the northern part of the quarry, joints are vertical and are NW-SE- to E-W oriented whereas in the southern part, the joints are steeply north-dipping and have a NW-SE to WNW-ESE orientation. Also a minor population of NE-SW- to NNE-SSW joints has been observed.

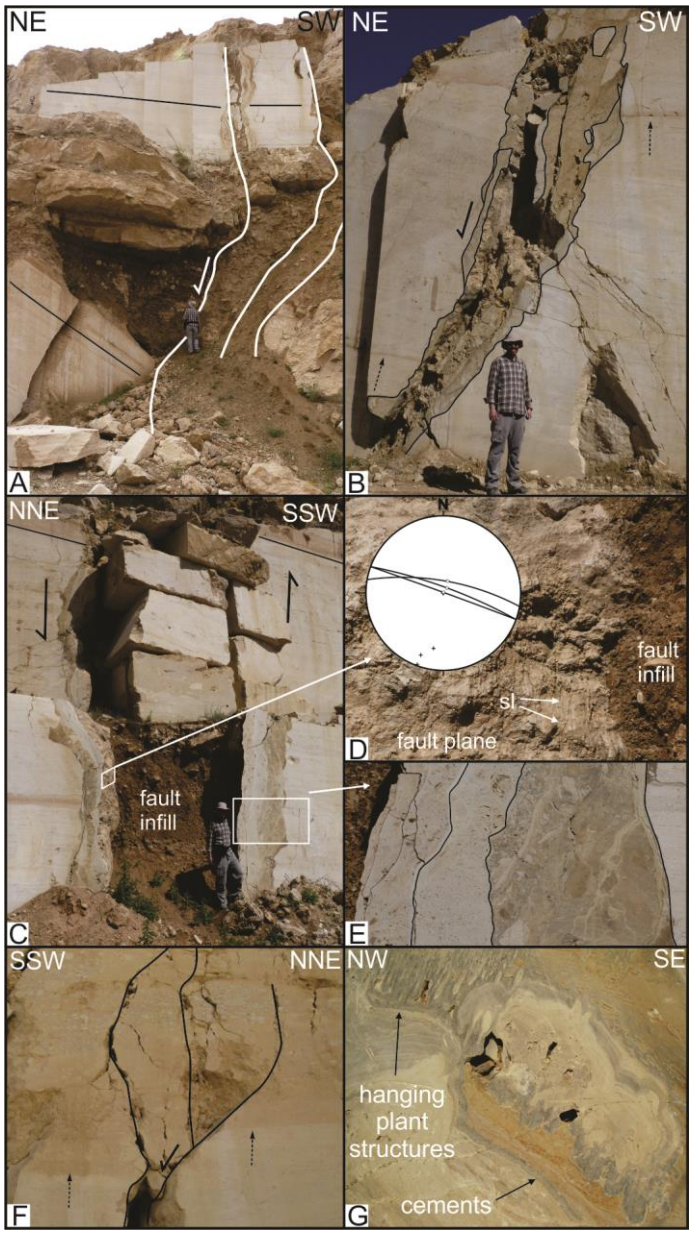


***Figure 5:*** *Kinematic features observed along of the Kömürcuoğlu faults.* ***A)*** *Interfingering marls and sandstone layers in the southern part of the quarry. Note the change in fault orientation when it hits the contact between clastic sediments and travertine.* ***B****) Northwards displacement of a normal fault in the S part of the quarry.* ***C & E)*** *Open normal fault in the S part of the quarry. Fault walls are characterized by a complex build-up indicative of multiple phases of faulting, lateral fluid flow and brecciation. The fault is filled by mud and travertine blocks.* ***D)*** *Dip-slip slickenlines (sl) observed in the hangingwall of the fault in c).* ***F)*** *Contact between travertine and conglomeratic cover. Southwards displacement of an N-dipping normal fault in the northern part of the quarry.* ***G)*** *Stalactite-like features hanging from a cave's ceiling. Cavity infill by cement precipitation of hanging plants observed in the small quarry (S. quarry). Cement infill around the cave.*

The **Pamukkale** and **Gama** quarries are excavating the hill north of the cement factory (Fig. 3). Based on bedding and on morphology of the mountain flank, a WNW-ESE trending domal structure can be recognised with a NNE- and SSW-dipping flank (Fig. 6A-A'). Faults are absent in the Gama quarry. In the Pamukkale quarry, several small, decimetre-scale displacement normal faults cut the abundant thin paleosols that are present in the laminated travertine. Faults are vertical to steeply N- and S-dipping and have a NW-SE trending orientation. This orientation slightly deviates from two large SW-oriented normal faults that limit the southern edge of the Pamukkale travertine. The travertine in the hangingwall of these faults is tilted with bedding steeply SW-dipping (~45°) (Fig. 6A-A', D).

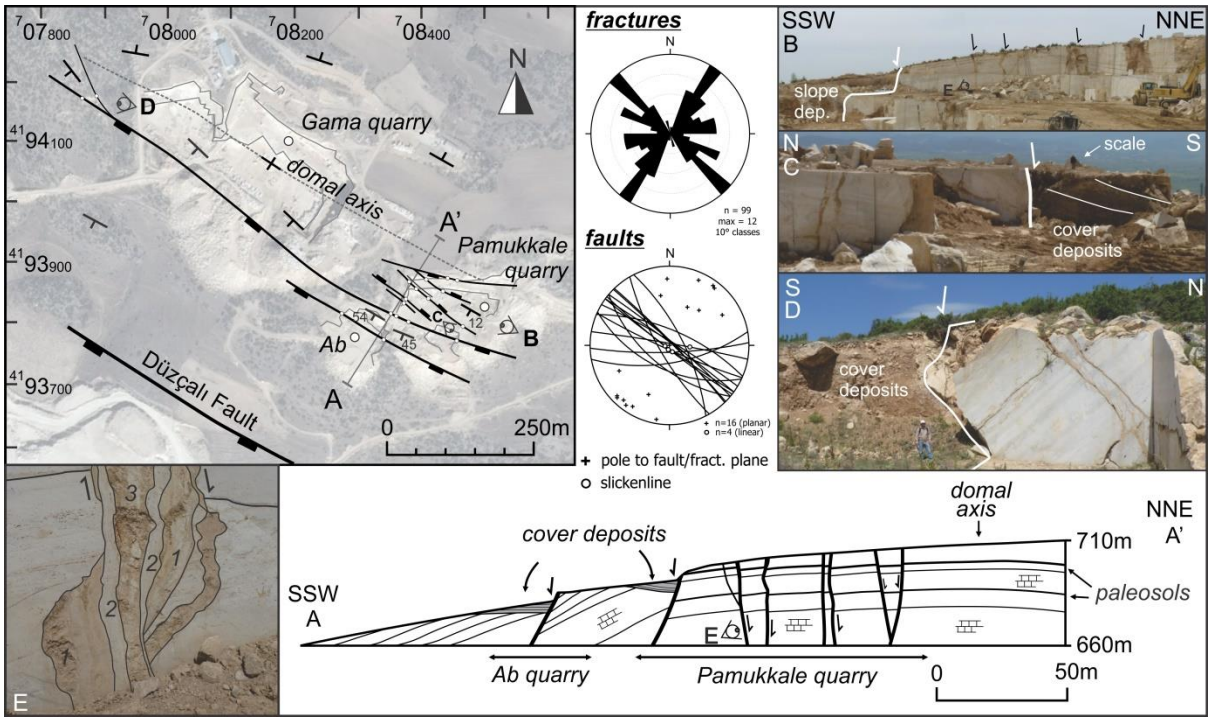


***Figure 6:*** *Fault map (basemap © Google Earth) and kinematic analysis (stereoplots) of normal faults observed in the Pamukkale and Gama quarries (NE Ballık area).* ***A-A')*** *The travertine is cut by normal faults.* ***B)*** *Overview of the Pamukkale quarry and minor normal faults.* ***C-D)*** *Two normal faults cut the edge of the Pamukkale-Gama travertine dome. Note the abrupt change of travertine into slope deposits or marls.* ***E)*** *Complex fault with several deformation and infill phases.*

Gravity-driven, fan-apron slope deposits, including unsorted, irregularly-oriented travertine blocks set in a sandy to marly matrix, cover the hangingwalls of these normal faults (Fig. 6B-D). The slickenlines observed on fault slip planes in these cover deposits are random in orientation indicating the ductile nature of the marls. These two faults can be followed through the quarry in a NNW-SSE direction. Fault history is characterised by numerous different stages of fracturing, fluid flow, brecciation and mechanical friction creating slickenlines (Fig. 6E). Joint population can be subdivided in three distinct, mutual abutting joint sets which are oriented WNW-ESE (parallel to the observed faults), NNE-SSW and E-W.

### *4.3 NW extensional domain: Kepez and Taşkestik Tepe*

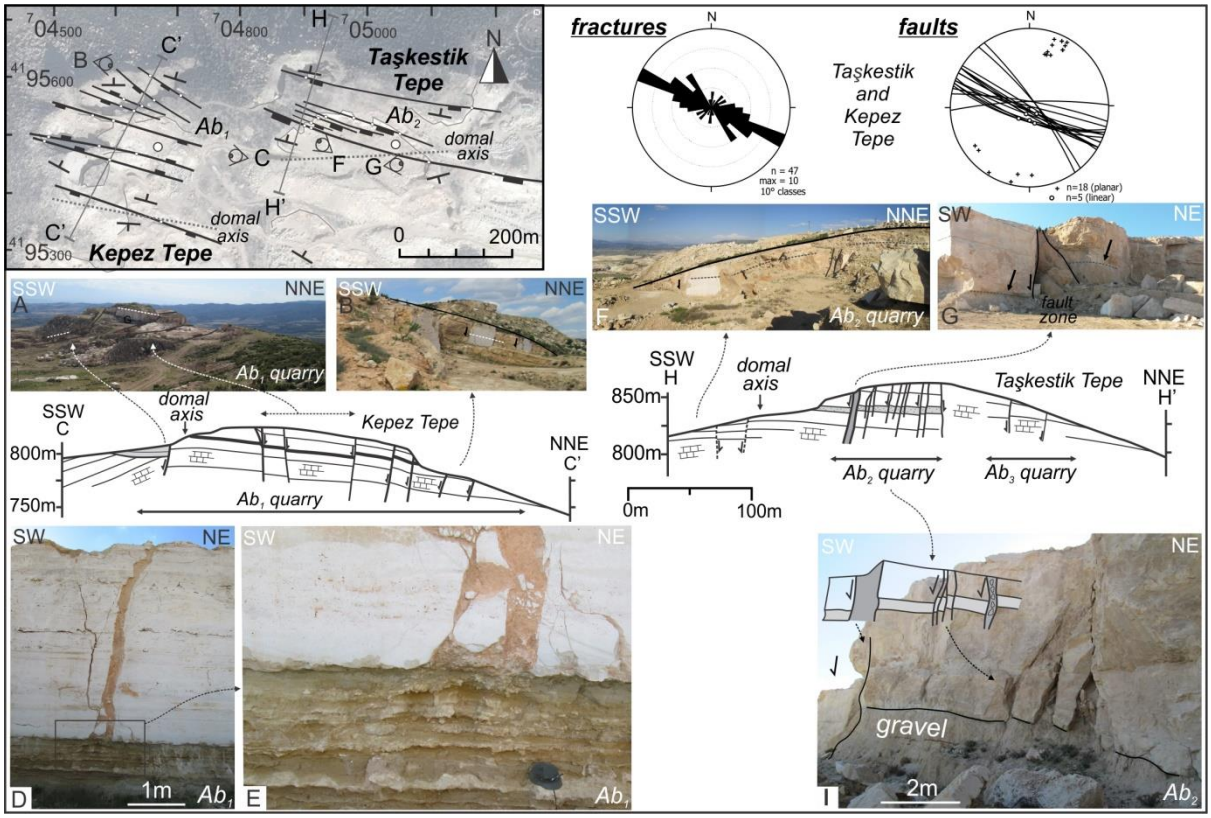


***Figure 7**: Fault map (basemap © Google Earth) and fault/fracture kinematic analysis (stereoplots) of the Abandoned quarries on the Kepez Tepe and Taşkestik Tepe. **C-C')** Normal faulting through the travertine on the Kepez Tepe. Note the change in bedding orientation due to activity along the SSW-most normal fault (**A)** and the NNE-dipping bedding in $Ab_1$ (**B**). **D-E**) Dissolution-enlarged and clay-filled fracture cutting the travertine but arresting on the gravel-travertine contact. **H-H')** Graben-facing normal faulting affecting the travertine on the Taşkestik Tepe. Note the 10 m displacement of a thick intercalating gravel layer at the SE end of the picture **I**.*

At the highest point of the northern graben edge, the **Kepez Tepe** and **Taşkestik Tepe**, two individual travertine domal bodies, are exposed (Fig. 7). In the NW, a WNW-ESE oriented travertine body was excavated in an abandoned quarry ($Ab_1$). Travertine dips gently to the NNE and is cut by WNW-ESE oriented normal faults (Fig. 7C-C'). Displacement is mostly to the SSW, however, in the middle of the quarry two faults have a NNE displacement. At the southern end of the travertine mass in $Ab_1$, bedding is dipping moderately to SSW due to block rotation along a listric normal fault (Fig. 7C-C').

A metre-thick gravel layer is present in the travertine. Joints are only limited to the travertine and arrest at the travertine-gravel boundary. The thick muddy infill of these joints (Fig. 7D, E) suggests that joints are dissolution enlarged by weathering of the fracture walls.

The travertine dome on the **Taşkestik Tepe** is also WNW-ESE oriented and was excavated in old abandoned quarry ($Ab_2$). Travertine dominantly dips to the NNE due to block rotation. At its lateral end, gently SSW-dipping layers are exposed (Fig. 7F, H-H'). SSW-facing normal faults affect the dome and can have displacements up to 10 m. Normal faults are consistent in orientation and can be traced for several hundred metres through the different quarries on the Taşkestik Tepe. Joint orientation is dominantly parallel to the faults.

### *4.4 Eastern extensional and strike-slip reactivated domain: Karakurt, Stone Terroir, Reisoğlu, and Özaş quarries*

In the Karakurt, Özhan and Stone Terroir quarries a continuous NW-SE oriented, subhorizontal travertine mass is excavated. NE of Karakurt, this travertine mass continues in the small valley of the Domuz river in which bedding alternates between gently NE- and SW-dipping (NE corner in map on Fig. 8). In the four quarries that are described next, the NW-SE oriented fault and joint set is the dominant one.

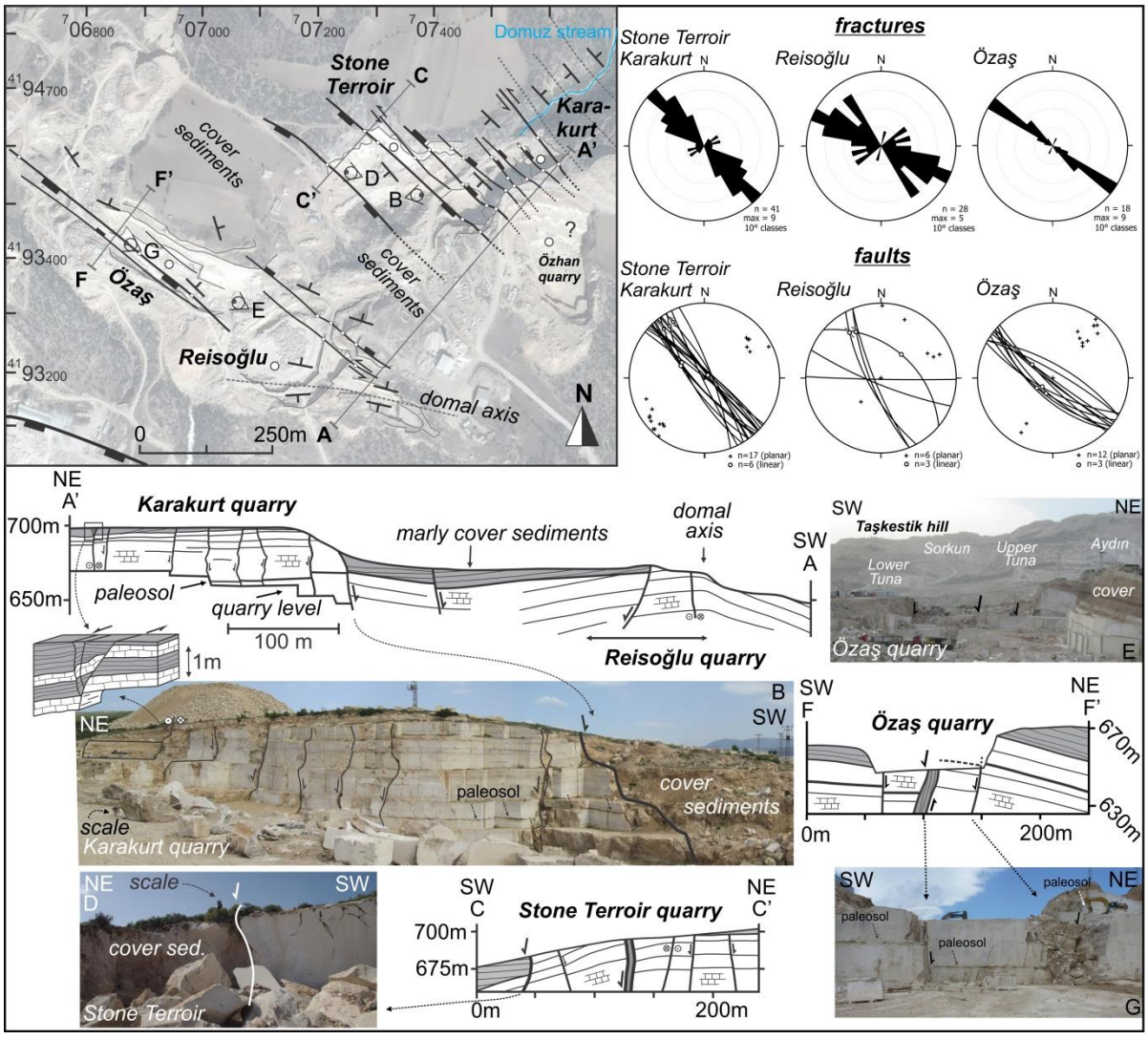


***Figure 8:*** *Fault map (basemap © Google Earth) and fault/fracture kinematic analysis (stereoplots) of Karakurt, Stone Terroir, Reisoğlu and Özaş quarries.* ***A-A')*** *Cross-section through Karakurt (**B**) and Reisoğlu quarries. In the NE part of Karakurt, a sinistral (transtensional) strike-slip fault with horizontal striae is present.* ***C-C')*** *Structure of Stone Terroir quarry. Large normal fault at the SW edge.* ***D)*** *Slope deposits cover the hangingwall.* ***E)*** *A marly-sandstone sequence covers the Karakurt-Stone Terroir and the Özaş-Reisoğlu travertine bodies.* ***F-F')*** *A wide SW-dipping normal fault zone with more than 20 m displacement cuts the NNE-dipping Özaş travertine mass. A 0.5 m-thick paleosol (**G**) and the marly-sandstone cover are displaced over 20 m by this fault.*

Subvertical NW-SE to NNW-SSE normal faults with decimetre- to metre-scale, alternating NE and SW displacement cut the travertine body in **Karakurt**. The NE part of Karakurt is cut by a

south-dipping strike-slip fault. Based on the slickenlines, slickensides and the observed displacement, a left-lateral fault movement can be deduced. The SW edge of Karakurt is cut by a SW-dipping normal fault (Fig. 8B) that can be connected to a 5m-wide, open fault zone in the centre of Stone Terroir (Fig. 8C-C').

In **Stone Terroir**, bedding changes from subhorizontal (lateral equivalent of Karakurt) to gently SW-dipping (~15°), forming the SW edge of the Karakurt-Özhan-Stone Terroir travertine mass. Fault infill is marked by subhorizontal slickenlines indicative of small-displacement strike-slip faults. The SW edge of the travertine body is cut by a SW-dipping normal fault (Fig. 8C-C', D). The travertine in the hangingwall of this normal fault is covered by deposits consisting of muds, marls and rotated travertine blocks (Fig. 8D). Marly deposits cover the travertine domes of Stone Terroir and Özaş. Between both quarries these cover deposits are expressed in the landscape as a flat field (Fig. 8F-F').

In the upper levels of **Reisoğlu**, a domal axis is visible with bedding oppositely NNE- and SSW-dipping (Fig. 8A-A'). This travertine body can laterally be followed towards **Özaş** where only the NE-dipping flank is excavated. A long SW-dipping normal fault is present in the centre of Özaş. This large normal fault has a c. 20 m SSE-oriented displacement deduced from a 0.5 m-thick paleosol (Fig. 8E, F-F'). Opposite to this normal fault, a smaller subvertical fault with a NE displacement is present (Fig. 8G) showing that the travertine in the centre of the Özaş quarry was collapsed due to extension.

### *4.5 Western extensional and strike-slip reactivated domain: Aydın, Sorkun, Simersan, Tuna and Emek quarries*

At the foot of the Taşkestik Tepe, the Sirmersan, Sorkun, Upper Tuna, Aydin, Sorkun Ab., Faber Ab. quarries excavate(d) a continuous NW-SE oriented 1.5-km long travertine geobody. Upper Tuna encompasses three travertine facies, which change from bottom to top from a subhorizontal facies interfingered with detrital channel facies to a waterfall facies. In Aydın and Upper Tuna travertine dips gently to the SSW (Fig. 9A-A'). In Upper Tuna, bedding is dominantly subhorizontal, whereas in the southern part of Upper Tuna and in Sorkun travertine dips gently to the NE. The top of the Sorkun and Upper Tuna travertine is covered by clastic sediments that can be interpreted as a siliciclastic channel facies consisting of fluvial conglomerates and marl sediments that wedge with the subhorizontal travertine facies. The terrace morphology of the Taşkestik Tepe is controlled by these channel sediments with flat horizontal fields indicative of siliclastic sediments, and steep hills indicative of travertine.

**Aydın** is characterised by three, meters-wide, WNW-ESE-oriented fault zones (Fig. 9B, C) filled with mud and travertine blocks. Slickenline orientation ranges from subhorizontal with a NW-SE trend, to gently SE- and NW-plunging, indicative of strike-slip and oblique-slip faulting.


***Figure 9:*** *Fault map (basemap © Google Earth) and kinematic analysis (stereoplots) of faults in the Emek, Lower and Upper Tuna, Aydın, Sorkun and Sirmersan quarries (NW Ballık area).* ***B & C)*** *Metre-wide, open strike slip fault zones with gently plunging slickenlines in Aydin.* ***D)*** *Block rotation in Upper Tuna.* ***E)*** *SW edge of the Tuna travertine mass which is bordered by a m-wide normal fault.* ***F-F')*** *Emek cross-section.* ***G)*** *Closely-spaced strike-slip faults in Emek.* ***H)*** *Overprinting strike-slip striae on fault infill.* ***I)*** *Normal faulting in Emek Ab. J) SW- edge of Emek Ab. where sandstone layers cover the Emek travertine mass.* ***K)*** *Precipitation along fault planes.* ***L)*** *Normal faulting in Emek.*

559 Slickensides indicate left-lateral faulting. Travertine block rotation inside the fault zones are
560 exemplified by slickenlines on internal fault slip planes (see grey great circles of slip planes in the
561 Aydın stereoplot in Fig. 9). Along-strike several fault bifurcations occur. This 600 m long fault zone
562 can be traced from the upper part of Aydın to the SE end of Sorkun Ab. The NW end of this strike-
563 slip fault zone can be traced through the landscape as its prolongation forms the transition between the
564 flat field NE of Sorkun and the steep flank at the foot of the Taşkestik Tepe.
565 Most normal faults in the upper Ballık area are SW-facing towards the graben floor. Between
566 Aydın and **Upper Tuna**, however, two steeply, NE-dipping normal faults occur (Fig. 9D). Bedding
567 was tilted to a steep SW-dipping attitude (P207/50) due to small-scale block rotation along these
568 faults. Mechanical fault striations on polished fault planes indicate pure strike-slip faulting. Two joint
569 sets are present in Upper Tuna. They are NNE-SSW to NE-SW and NW-SE oriented, congruent to the
570 two fault populations in this quarry.
571 In **Sorkun**, several short strike-slip faults with a brecciated fault core developed in a flat-pool
572 travertine facies. Left-lateral fault movement is deduced from slickensides and mineral growth in fault
573 planes. Joint orientation is very irregular in the Sorkun quarry. The regional NW-SE joint set is still
574 present, but also other moderately dipping joint sets cut the travertine.
575 In **Sirmersan**, two small travertine bodies are excavated. Bedding often changes internally as
576 the travertine typically consist of gentle slope-dominated facies. These bodies are covered by a marly
577 sedimentary unit that continues northwards to the base of the Kepez Tepe. The travertine is cut by rare
578 strike-slip faults and by one N-facing normal fault with a thick fault infill. NW-SE and E-W joints are
579 the most abundant.
580 In the **Emek** quarry and in its abandoned part (**Emek Ab.**), travertine dips gently to the NNE
581 and consists mainly of a flat-pool facies. Faults are consistently parallel and have a steeply SW-
582 dipping attitude (see stereoplots in Fig. 9). This orientation is also represented by the joint population
583 in which the majority dips steeply to the SW. The northern part of Emek travertine is cut by three
584 strike-slip faults (Fig. 9G). The northernmost fault forms the NE excavation front of the quarry and is
585 filled with a coloured mud rich in iron (brown) and manganese (black) oxi/hydroxides (Fig. 9H).
586 Gently (L100/20) to moderately ESE-plunging (L130/40) slickenlines, indicative of strike- and
587 oblique-slip, respectively, overprint steeply-plunging striae (L230/80). Paleosol displacements along
588 SW-dipping fault planes (P210/80) containing NW-plunging slickenlines (L302/05) indicate a
589 sinistral strike-slip deformation. In the centre of the active Emek quarry, several parallel, closely-
590 spaced (20 m spacing) normal faults are present (Fig. 9F-F', G). The largest normal fault is a 3 m-
591 wide open fault that is filled by mud and travertine blocks and which can be traced along-strike to
592 Emek Ab. A 20 m normal displacement can be estimated based on the displacement of a thick
593 paleosol (thick black line in Fig. 9F-F', L) and by dip-slip slickenlines plunging to the SW (L210/55).
594 Similarly to observations in other quarries, faults had an open nature in which circulating fluids
595 precipitated as carbonate cements along fault planes (Fig. 9K).

**Emek Ab.** is bordered in the SSW by a hectometre-long fault zone. Travertine bedding in the footwall is gently NNE-dipping. The hangingwall is composed of coarse-grained sandstone layers with a steeply SSW-dipping attitude (P232/62) (Fig. 9J). This sandstone is situated on a higher stratigraphical and structural position than the Emek travertine body and represents an interfingering clastic facies.

The 20 m-displacement, normal fault zone crossing the Emek travertine continues towards the **Lower Tuna** quarry. Here, travertine dips gently to the NNE and marl and mud deposits cover the hangingwall of this wide fault zone (Fig. 9A-A', E). The northern NE-dipping fault wall (P040/81) is marked by WNW-plunging slickenlines (L300/48), indicative of normal faulting with a substantial oblique-slip component.

### *4.6 Strike-reactivated domain in the footwall of Düzçalı fault: the Best Shear Zone, Faber W, Tetik and Özçınar quarries*

In the **Best** quarry and in two adjacent abandoned quarries ($Ab_1$ and $Ab_2$ in Fig. 10), travertine dips to the S, SE and SW and deposition took place along an already developed gentle slope (slope facies. Numerous parallel, closely-spaced, NW-SE to WNW-ESE-trending strike-slip faults (Fig. 10A, B-B') can be traced through the Best quarry. Owing to a dense fault spacing, this part of the northern graben flank is further referred to as the Best Shear Zone. The often metre-thick sedimentary fault infills consist of brown, chaotically-ordered oxidised muds, small travertine blocks and organic-rich material (Fig. 10C-E). Successions of paper-thin, brittle, calcite rafts are present in the fault, indicating that during fault development circulating fluids stagnated for a certain period in the open fault (cf. El Desouky et al. 2014; Fig. 10D). The fault planes are coated by white to brown calcite cements giving them a nodular-shaped appearance. Slickenlines and slickensides are mostly only present on the polished cemented nodule-shaped surfaces and on the muddy fault infill, but never as mechanical striations on the travertine rock itself (Fig. 10F). Mineral steps on the slickensides all indicate left-lateral shear suggesting that strike-slip faulting occurred after fluid flow along the fault planes.

In the northern part of Best (Fig. 10G), the NW-SE fault orientation deviates from the dominant WNW-ESE fault orientation found in the entire Ballık area. In this part, also two shear zones are found (Fig. 10H) in which fault walls are marked by slickenlines and in which the internal part consists of metre-large rotated travertine blocks. Only two minor normal faults parallel to the orientation of the adjacent strike-slip faults, are present.

Joint sets show a large variety in orientation. Joints are parallel to the WNW-ESE faults, but also an apparent dominant ENE-WSW joint set is present in the Best quarry. Considering the small angle (~50°-70°) between both joint sets, they could reflect conjugate jointing during shear deformation.

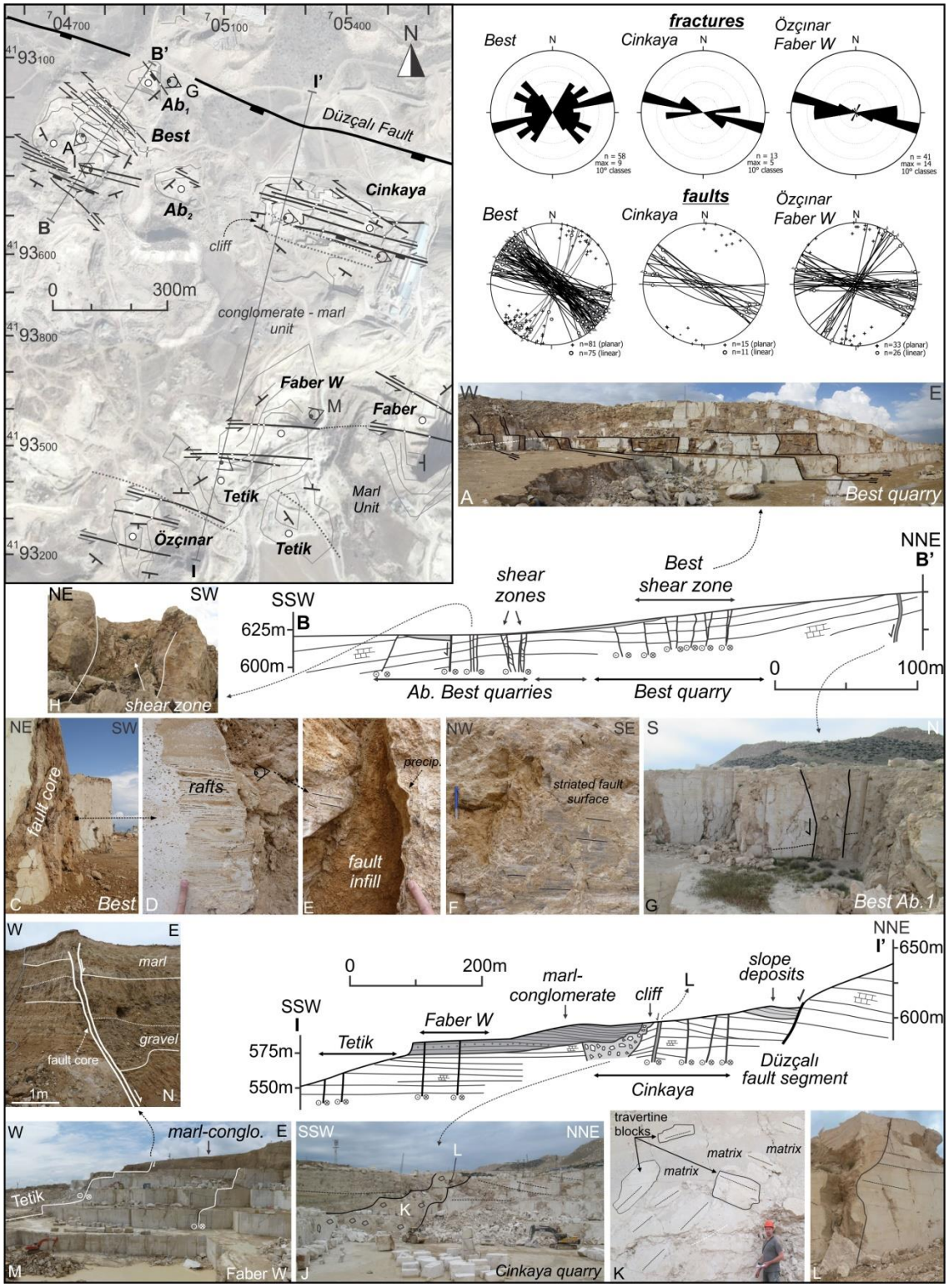


**Figure 10:** *Fault map (basemap © Google Earth) and fault/fracture kinematic analysis (stereoplots) of the Cinkaya, Best, Faber W, Tetik and Özçinar quarries (NW lower Ballık area).* ***A)*** *NW-SE to WNW-ESE strike-slip faults in the Best quarry.* ***B-B'****) Best shear zone Cross-section .* ***C)*** *Shear Zone fault core.* ***D-F)*** *Disrupted muddy fault infill, successions of thin, brittle rafts and cementation/precipitation along the fault wall. Striated polished nodular-shaped fault wall in E.* ***G-H)*** *Open faults with infill of travertine blocks.* ***I-I'****) Düzçalı Fault to Tetik quarry cross-section showing NNE-dipping travertine in Cinkaya and subhorizontal facies in Faber W and Tetik. Cinkaya travertine is bordered by the Düzçalı fault.* ***J)*** *The marl-conglomerate layer (also discussed in Claes et al., 2015) starts from a cliff (****L****) and covers the travertine of Faber W and Tetik. K) Floating travertine blocks floating in a muddy matrix.* ***M-N)*** *Strike slip faults in Tetik and Faber W. continuing through the marl-conglomerate layer covering the travertine excavated in Faber W.*

In the **Cinkaya** quarry, bedding is subhorizontal in the middle part, NNE-dipping in the northern part and SSW-dipping in the SW part of the quarry and deposited as a flat pool facies. Along the western quarry flank, the SE-dipping travertine mass is abruptly cut by a steep, stepwise erosional cliff (Fig. 10I-I', J, L). A debris layer covers the travertine along the southern edge of this cliff. In this debris layer, large travertine blocks are irregularly piled up and are 'floating' in a fine-grained travertine matrix (Fig. 10K). The debris layer can be laterally traced through Cinkaya in a WNW-ESE direction. Similar cliff-like structures are described along the Honaz fault zone where they are exposed as fault scarps along major fault segments segments (Koçyiğit, 2005). These similarities suggest that the cliff in Cinkaya represents an ancient, synsedimentary inactive fault.

The Best Shear Zone can be prolonged towards Cinkaya where WNW-ESE strike-slip faults with left-lateral strike-slip kinematic indicators on the fault infill are observed. On a normal fault in the centre of Cinkaya, steeply-plunging slickensides are overprinted by subhorizontal slickenlines indicating that normal faults are strike-slip reactivated. Joints are consistently parallel to the mapped faults.

The marl-conglomerate alluvial plain unit, of which the debris layer forms the base, continues to the south, where it reaches a thickness of 20 m. It covers the **Faber W** travertine mass (Fig. 10M) and thins out to the east in the Faber quarry (i.e. referred to as the marl-conglomerate occurrence in Claes et al., 2015) where it covers the subhorizontal travertine facies in the lower levels of Faber and Ece quarries.

Joints and faults in **Faber W**, **Tetik** and **Özçınar** show a dominant WNW-ESE orientation (Fig. 10) and consist of a flat pool facies. Fault walls are marked by subhorizontal E- to W-plunging subhorizontal slickenlines with sometimes clear left-lateral slickensides. N-S-trending slip planes often can be observed in the fault infill (see plots of Faber W in Fig. 10). In the sedimentary marl-conglomerate cover, a normal, northwards-oriented displacement of 2 m has been observed (Fig. 10N). Evidence of post-sedimentary faulting are clay smearing of the incompetent marly layers inside the fault zone and thickening of a conglomerate layer at the intersection of the fault and the antithetic fault. Clast rotation (cf. Loveless et al., 2011) cannot be observed due to the fact that clasts are spherical. Inside the travertine mass, subhorizontal left-lateral strike-slip kinematics are found along the fault wall of the same fault, indicative of fault reactivation.

### *4.7 Killik domal area and Southern Ballık area*

Tectonic deformation and development of the fault/fracture network affecting the Killik domal area (Faber, Ece, Tetik, Çakmak, İlik, Alimoğlu and Best Ab. Quarries, see Fig. 2) have been extensively studied by Van Noten et al. (2013). Other researchers have studied the complex sedimentological build-up of travertine (Özkul et al., 2013; Claes et al., 2015; De Boever et al., 2016; De Boever et al., 2017) and detritic intervals in these quarries. The Killik dome continues towards the east where it is excavated by the Alimoğlu Tasarim, Denmer, Başaranlar, Metamar and Şiray quarries.

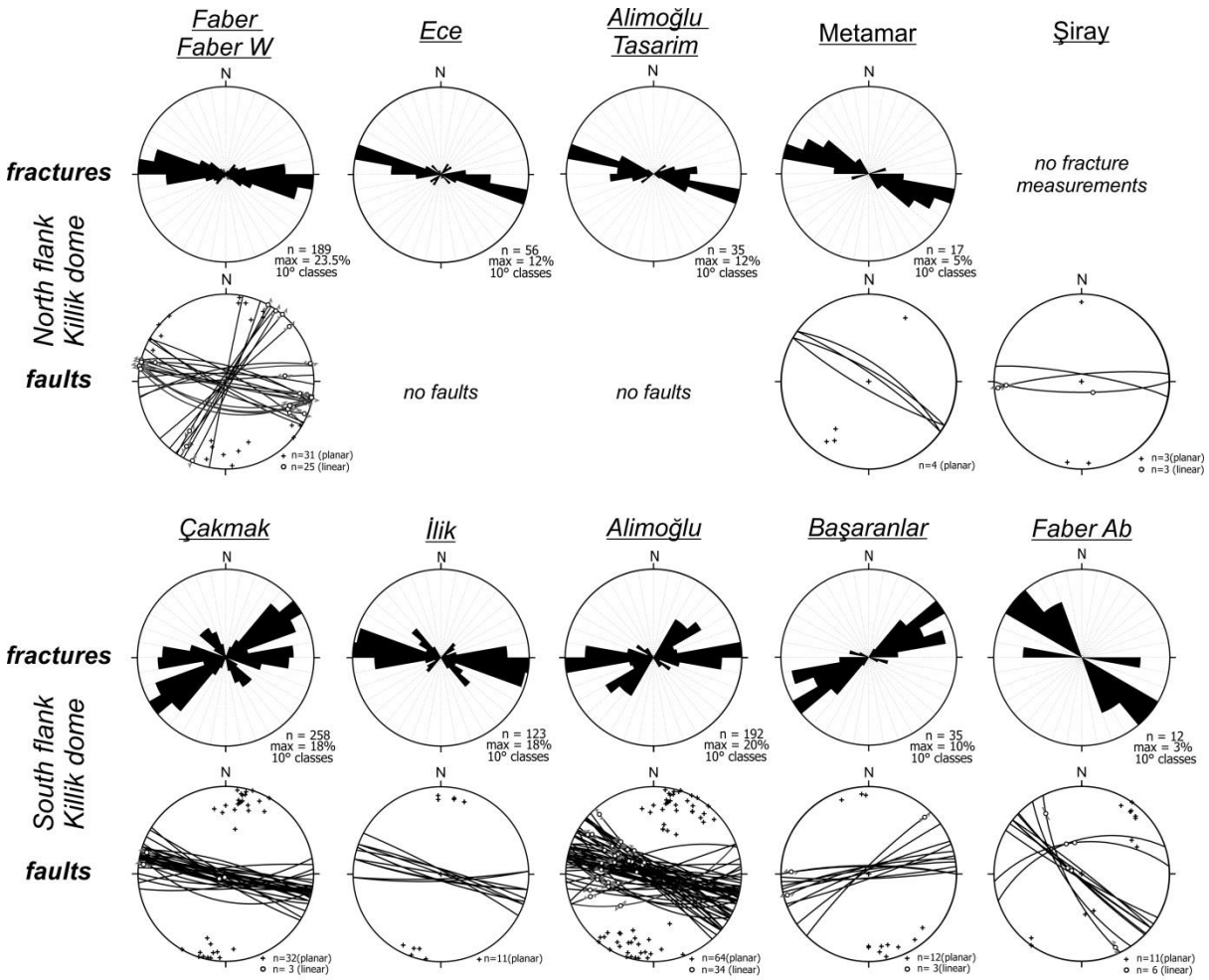


***Figure 11:*** *Fault and fracture orientation analysis (stereoplots) of the Killik dome. See Fig. 2 for quarry locations. Rose diagrams illustrate fracture distribution. Northern and Southern flanks of the Killik are separated.*

Along the northern flank of the Killik dome (**Alimoğlu Tasarim, Metamar)** travertine is mostly subhorizontal and is covered by a thick marl-conglomerate facies. Alimoğlu Tasarim is dominated by joints that bifurcate in the cover sediments. In Metamar (Fig. 11), NW-SE normal faults are parallel to the Düzçalı fault and have NE- and SW displacements, creating a mini-graben in the Metamar quarry.

The travertine in the SW part of the Killik dome (Çakmak, İlik, Alimoğlu and Best Ab) changes from horizontally bedded at the base towards a more complex low-angle slope facies near the upper part. The eastern domal part (**Denmer, Başaranlar** and **Şiray**), however, consists of subhorizontal bedded travertine dipping gently to the SSW and SSE. The fact that the complexity of the Killik dome does not continue towards the east, suggests that either other major sources may have been present to cause the formation of the travertine in Denmer and Başaranlar or that these travertines formed in a later timing and different flow path but from the same spring location. E-W oriented normal faults cut the edge of the travertine in Başaranlar. In Şiray, faults are also E-W oriented and show evidence of both normal and strike-slip faulting.

Few abandoned quarries (**Faber Ab.**) are present in the area below the cement factory and north of the Killik fault. Here, a small, NW-SE oriented domal structure, with opposite NE- and SW-dipping flanks is present. Based on the orientation of this structure and the absence of any connection with the Killik dome, a different source can be assumed. This travertine mass is cut by several NW-SE oriented normal faults with subhorizontal slickenlines on the fault infill.

Contrary to the tilted blocks along the northern flank of the DGHS, the Killik dome is not affected by block tilting. Faults have a different orientation along both flanks of the Killik dome. Whereas NW-SE oriented faults cut the northern flank, E-W to WNW-ESE faults affect the southern part. This is for instance exemplified by the difference in fault orientation in Şiray and Metamar. Based on fault distribution, the rigidity of Killik dome thus seems to have played a role in such way that faults preferentially developed along its flanks after travertine formation but hardly in its centre. A major fault feeder system responsible for the travertine deposition of the Killik dome has not been found but based on slope analysis it should be located along the domal axis between the Çakmak - İlik - Alimoğlu (the southern domal flank) and the Faber – Ece - Alimoğlu Tasarim quarries (the northern domal flank).

In the Killik dome, fracture propagation is influenced by the different travertine facies. Joints that developed in subhorizontal travertine facies are continuous and straight, whereas joints in slope facies have an irregular trace and are affected by the local travertine bedding forming staircase fractures (cf. Maggi et al., 2015). In the northern flank of the Killik dome, i.e. in the NNE-dipping and subhorizontal flanks, joints are dominant WNW-ESE oriented and are parallel to the mapped normal and strike-slip faults affecting this part (Fig. 11). As the northern part is situated in the hangingwall of the Düzçalı fault, joints and faults show a large parallelism to the trace of this fault. In the eastern part of the Killik dome, i.e. in Çakmak, İlik and Alimoğlu, majority of the joints are parallel to the E-W to WNW-ESE oriented faults. Two other significant joint sets, i.e. a NW-SE and a NE-SW oriented set, can be recognised. Towards the eastern end of the Killik dome, joints in Başaranlar are NE-SW oriented and deviate slightly from the E-W oriented faults. Jointing could here be affected by the locally NE-SW trending Killik fault. In Faber Ab., fractures are parallel to the local faults and are dominant NW-SE trending.

# 5. Paleostress analysis

Paleostress inversion results in three orthogonal principal stress axes and the stress ratio $R = (\sigma_2 - \sigma_3) / (\sigma_1 - \sigma_3)$, which classifies the stress tensors as radial/pure/strike-slip extensive, extensive/pure/compressive strike-slip or strike-slip/pure/radial compressive stress states. Inversion is sometimes problematic if the observed deformation results from multiphase deformation history and if fault data is heterogeneous (e.g. Çiftçi and Bozkurt, 2009). To overcome this problem, in this study, faults observed in different quarries but that have similar kinematics were grouped. To identify

different fault populations and stress orientations, we rejected faults with high misfit angles in the Win_tensor Program until a solution with homogeneous faults was found. When a rejected fault population resembles faults in neighboring quarries, then this population was regrouped into a new subset for which the inversion was rerun. The stress regime index R' distinguishes between pure extensive, transtension and a pure strike-slip regime (Fig. 12).

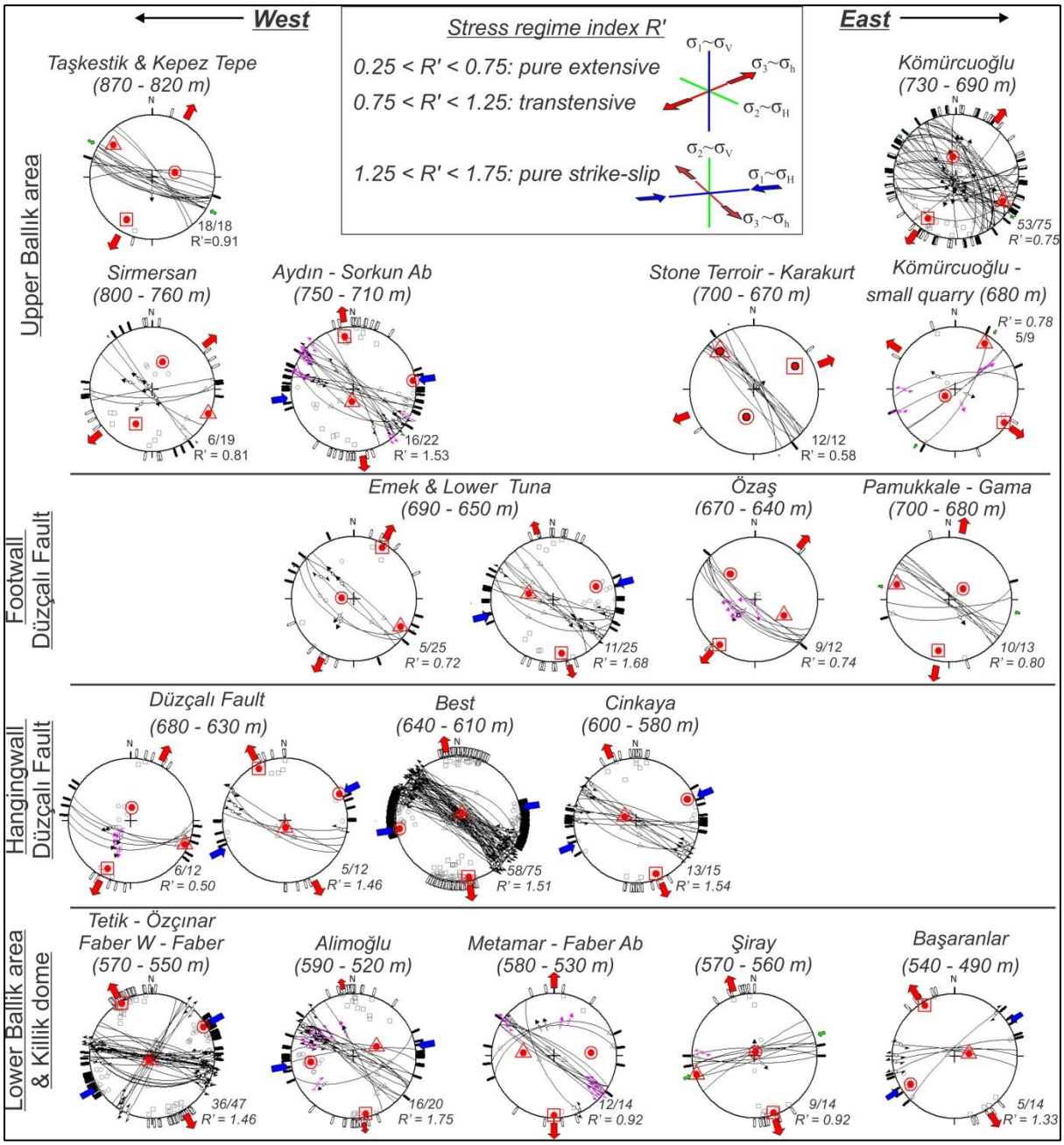


***Figure 12:*** *Stress inversion of selected fault data and associated slip planes observed in the Ballık area illustrated in lower-hemisphere equal area stereoplots. Quarries are ordered from west to east in different domains according to the elevation and tectonic blocks in which they occur. Stress inversion results in the three principal stress axes (circle for $\sigma_1$, triangle for $\sigma_2$ and square for $\sigma_3$). Number of used fault-slip data with respect to the total amount of data for the considered fault data is indicated. Outward arrows indicate extensional deviatoric stresses; inward arrows represent compressional deviatoric stresses. Blue arrows: $\sigma_1$ ($S_{Hmax}$). Green arrows: $\sigma_2$ ($S_{intm}$). Red arrows: $\sigma_3$ ($S_{hmin}$). In some quarries (Emek, Lower Tuna, Şiray, Başaranlar and Düzçalı fault) two stress regimes (NNE-SSW extension and WNW-ESE strike-slip faulting) are deduced. The Düzçalı fault inversion results from fault data gathered in this study and from Koçyiğit (2005).*

Paleostress inversion carried out on the fault data results in two dominant but significantly different stress regimes: NE-SW pure extension (R' < 0.75) to transtension (0.75 < R' < 1.25) and a pure strike-slip regime (1.25 < R' < 1.75) with ENE-WSW compression and NNW-SSE extension. The northeastern (Kömürcüoğlu, Pamukkale, Gama, Stone Terroir, Karakurt) and northwestern (Kepez and Taşkestik Tepe, Sirmersan) areas were only affected by NE-SW extension to transtension (= oblique opening). Travertine at the base of the Taşkestik Tepe was strongly affected by the strike-slip regime.

Locally in the small quarry south of Kömürcuoğlu, the deduced NW-SE extension deviates from regional extension. Because of the local presence of the NE-SW transfer zone between the Düzçalı and the Elmalı faults in this region (Fig. 2), this NW-SE extension might be a local effect and cannot be extrapolated to a regional stress regime.

Travertine in the footwall of the Düzçalı fault and this fault itself bear characteristics of both the NE-SW extension regime (Emek, Özaş, Lower Tuna, Pamukkale, Gama, Düzçalı) and the strike-slip regime (Emek, Emek Ab, Lower Tuna, Düzçalı). Stress inversion of fault data in the lower part of the Ballık area (Tetik, Özçınar, Faber W, Faber, Alimoğlu, Başaranlar) results in the strike-slip regime. Strike-slip kinematics are absent in the middle part of the Killik dome (Metamar, Şiray). Stress inversion shows a slightly different extensional direction with N-S extension.

The NE-SW to NNE-SSW extension that deformed the Ballık area clearly shows a congruence with the current Holocene NE-SW to NNE-SSW extension in the eastern and central parts of the DGHS, as indicated by focal mechanisms of recent small to moderate earthquakes (Irmak, 2013) and kinematic analysis of the margin-bounding faults along the Denizli and neighbouring Grabens (Çiftçi and Bozkurt, 2009; Kaypak and Gökkaya, 2012).

# 6. Discussion

## *6.1 Travertine morphology*

Although a detailed travertine facies analysis is beyond the scope of this study, the general dip and morphology of the different studied travertine deposits can be used to identify the morphology of the Denizli margin at the time of Pleistocene Ballık travertine deposition and allows tentatively to locate possible feeder systems. Establishing this morphology is important to separate sedimentological depositional from tectonic deformation processes. In general, in the Ballık area, travertines occur as (large) travertine geobodies deposited in flat pools and in slope-controlled travertine mounds in the eastern part and as individual travertine domes in the western part.

The Kömürcüoğlu travertine body (Figs. 2 and 3) is oriented E-W, orthogonal to the orientation of the nearby travertines in the Ballık area. Based on facies occurrence and present and deduced paleo-topography, a large mound travertine geobody can be proposed, characterized by a

lobe geometry of different facies including subhorizontal, channelled pool terraces (cf. Violante et al., 1994) and biohermal reed facies (Fig. 13). Based on the oppositely sloping facies a second, agglomerative lobe was deduced in the SSW part of the Kömürcüoğlu quarry. The vertical change of sub-horizontal facies to channelled pool terraces facies (pools and barrages) is related to the increase in occurrence of higher plants (bryophytes, mosses, reed stems) in the pools. These plants make barrage bodies and impede water flow, causing changes in topography from East to West at Kömürcüoğlu. Higher in stratigraphy biohermal reed facies is formed, eventually leading to a sloping topography along which rapid water flowed and slope travertine facies developed. The increasing amount of higher plants (Fig. 5G) towards the top of the deposits represent a cooling and shifting water flow direction and eventually the formation of paleosol intercalations. Several metre-scale primary caves develop below hanging plants. Originally, the formation of these hanging plants should be driven by gravity and should have grown nearly vertically in biohermal reed facies. In southern Kömürcüoğlu quarry, however, these plant structures have a steep dip of ~70° (Fig. 5G). This observation indicates that this part of the travertine mass was rotated towards the SE, presumably by block rotation due to local faulting. At the end of the system travertine deposition ceased, which is demonstrated by alternation of finer mud sediments and less well-sorted matrix-supported conglomerates that cover the Kömürcüoğlu travertine. The detritals are products of cohesive debris flows (Nemec and Steel, 1984).

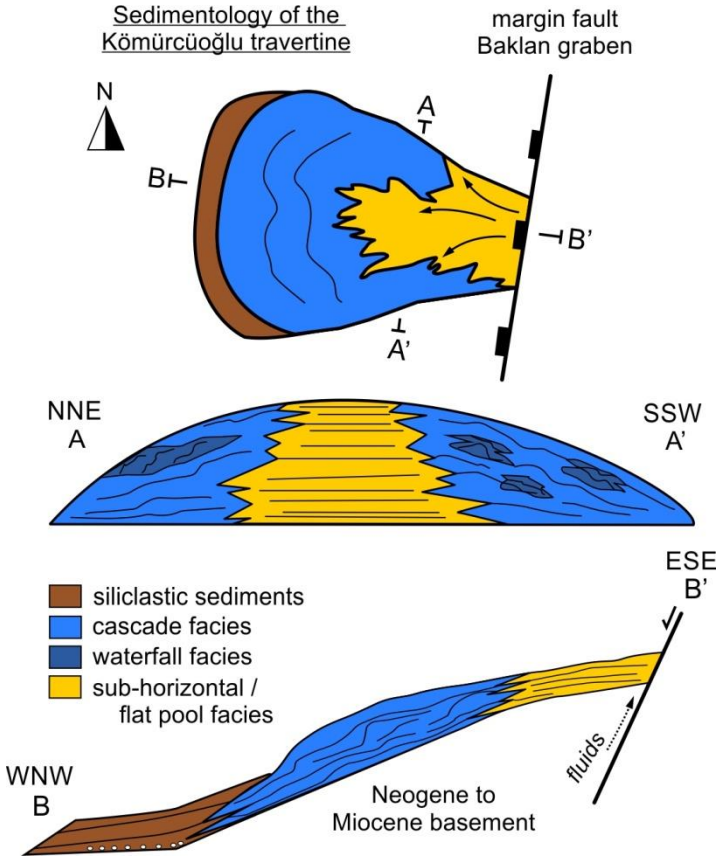


***Figure 13:*** *Simplified conceptual model and cross-sections of the geometry of the main travertine lobe of the Kömürcüoğlu travertine. Based on the lobe geometry, a travertine source WNW of the quarry is expected.*

The paleo-springs as source of the Kömürcüoğlu mound geobody should be found northeast of the Kömürcüoğlu quarry. Because the travertine geobody formed in alignment with the NE-SW trending fault system on the front of the fault-controlled Malıdağı mountain (Fig. 1), it is plausible that this fault, which is related to Baklan Graben development, acted as a source. Also north of Kömürcüoğlu (Fig. 1), the Belevi travertine system developed downslope and was sourced by the NE-SW trending graben-edge fault of the Baklan Graben (Claes et al., 2017b).

The travertine in the Killik domal area originated from meteoric fluids that have interacted with basement rocks at depth and emerged along the graben margin faults to the surface (Claes et al., 2015; El Desouky et al., 2015). The Killik dome is a depositional dome with horizontal to subhorizontal bedded travertine present in the lower part that gradually changes upwards to cascade/slope and waterfall facies travertine.

Travertine masses developed along the northern graben flank, i.e. the Pamukkale-Gama, Karakurt-Stone Terroir, Özaş, Emek-Lower Tuna and Taşkestik-Kepez Tepe travertines consist of WNW-ESE oriented (sub-)horizontal to gently S-wards sloping travertine masses (similar to the 'eroded-sheet travertines' of Altunel, 1994). As this subhorizontal travertine facies occurs north (footwall) and south (hangingwall) of the Düzçalı fault, a similar large normal fault system should be present at depth north of Düzçalı sourcing the necessary fluids for the large-scale observed subhorizontal travertine system . The extent of this fault system is unknown and can be hidden in the underlying Neogene unconsolidated sediments. Hence, sourcing potentially occurred diffuse through these sediments. This interpretation is supported by the fact that no banded travertines or central feeder system has been found in the Ballık area, thus suggesting a large depression as depositional environment (Fig. 14A). The good rock quality of the travertine masses in the upper part suggests that at the time of travertine deposition, already an uplifted mountain morphology must have been present to create subhorizontal to slope-dominated travertine facies that were not totally destroyed by further uplift of the mountain flank.

The fact that many siliciclastic sequences intercalate and cover (Fig. 14B) the different travertine masses along the northern margin suggests that a clastic source of sediments must have been located in the mountain range north of the Ballık area (Fig. 1). However, as the Taşkestik Tepe travertine is currently the highest point in the Ballık area, a considerable uplift of the Taşkestik Tepe occurred during the late Pleistocene-Holocene (Fig. 14C) shutting of the Ballık area from this clastic source.

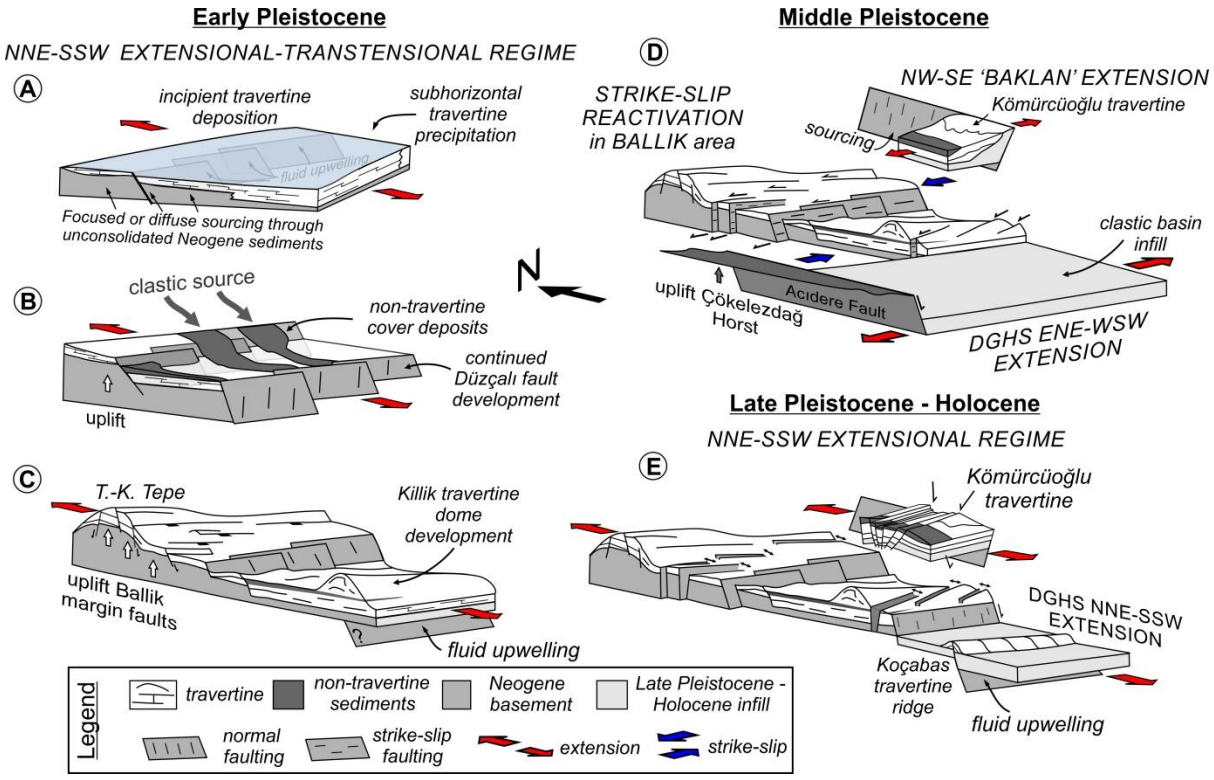


***Figure 14:*** *Conclusive cartoon (not to scale) illustrating the sedimentological and tectonic evolution of the Ballık travertine.* ***A)*** *Early Pleistocene subhorizontal travertine development on top of Neogene basement sediments/rocks.* ***B)*** *Alluvial system covering the travertine with marly and clayey sediments sourced from the mountain range north of the Ballık area.* ***C)*** *Normal faulting and uplift of the Taşkestik (T.-K) Tepe simultaneously with development of the Killik travertine dome.* ***D)*** *Kömürcuoğlu travertine development, sourced by the NNE-SSW trending Baklan margin fault. Baklan Graben and the DGHS in ENE-WSW extension. Normal faults in the Ballık area reactivated into strike-slip and acting as transfer zone between both regions.* ***E)*** *Collapse of the Ballık area with opening and infill of normal faults. Active travertine precipitation occurred further basin-inwards e.g. at Koçabas.*

### *6.2 A relative travertine age model*

With limited amount of age data available in literature, restoring a complete chronology of different travertine deposition along the entire northern flank remains enigmatic. However, geomorphological evidence, travertine architecture and fault crossing relationships can be used to constrain a tentative relative travertine age model (Fig. 14). Around the world numerous examples are known (e.g. Turkey, Hungary, off shore Brazil) in which inactive travertines are present at elevated levels, because they were cut off from the main water table due to tectonic uplift, and where active spring travertine precipitation has shifted to lower areas (e.g. González-Martín et al., 1989; Capezzuoli et al., 2010; Özkul et al., 2010; Özkul et al., 2013; Çolak Erol et al., 2015; Claes et al., 2017a; Wang et al., 2017). This also occurred in the DGHS as the Killik dome is younger than the travertine developed along the northern margin flank. Formation of the Killik dome occurred simultaneously when extensional deformation was affecting the already deposited travertine masses along the margin flank (Fig. 14C). Lebatard et al. (2014) concluded from paleomagnetism in combination with cosmogenic nuclide dating that the travertine in the lower part of the Killik dome ranges between 1.7 and 1.1 Ma. The

younger, upper parts date between 1.22 and 1.07 Ma (Lebatard et al. 2014) but might have younger ages as the uppermost levels have not been dated yet. The Taşkestik Tepe lies 260 m higher than the youngest part of the Killik dome. Taking a general uplift rate of 0.2 mm/a in Anatolia (Westaway et al., 2003) into account, then the earliest deposition along the Taşkestik Tepe could potentially date back to 2.5 Ma, i.e. Early Pleistocene (Fig. 14A). This age is probably overestimated as displacement related to normal faulting is not considered in the calculation and significantly contributed to the uplift, but it sets an age window in which travertine deposition needs to be framed.

U/Th depositional ages of the Kömürcüoğlu and Belevi travertines vary between 490±50 and 510±50 ka (Özkul et al., 2004), which is significantly younger than the Ballık travertine. Because both travertine masses are sourced from Baklan margin faults, this age suggest that the NE-SW 'Baklan' extensional stress regime must have been active during deposition of these travertine masses (Fig. 14D). With time the travertine deposition migrated from the northern graben flank to a more central part of the DGHS, e.g. at Koçabas (181 ka to 80 ka; Toker et al., 2014) (Fig. 14E).

### *6.3 Development of the extensional fault/fracture network*

In Western Anatolia, the Baklan, Acigöl, Dinar and Burdur Basins are all characterized by master border faults that progressively young and downtrow towards the depocentre in the basin. The seismogenic Dinar fault zone (Fig. 1b), for example, is subdivided in an outer and inner fault zone of which the former is characterised by Miocene-Pliocene strike-slip tectonics, whereas the latter formed by younger Quaternary normal tectonics (Alçiçek et al., 2013). Also the northern margin of the Denizli Basin (e.g. at Pamukkale) is characterised by a stepwise basin morphology that is dominated by normal fault segmentation (Kaypak and Gökkaya, 2012). Travertine formation is mainly associated to transfer zones between the stepwise NW-trending margin faults (Alçiçek et al., 2015) that also young towards the basin centre, a process which is accompanied by the development of different fluvial terraces (Özkul et al., 2013).

Also in the Ballık area, faults progressively young from the uplifted horst towards the basin centre. Hence, the paleostress regimes deduced from the fault kinematica can be used to reconstruct the deformation of the Ballık area. Because the Quaternary travertines are developed on loose Neogene sedimentary basin fills, there is a risk that the mapped faults do not resemble the regional tectonics. Indeed, some suspicious stress inversion results do not resemble the regional inversions but rather local gravitational collapse (e.g. the NW-SE extension in the Kömürcüoğlu small quarry in Fig. 12 can be linked to activity along the Killik fault). The majority of the stress inversions, however, all result in very similar stress regimes suggesting that the analysed directions are regional.

Similar to the northern graben margin of the Çürüksu Graben, the Ballık area is characterised by fault segmentation. From the Kepez Tepe quarry in the west to the Pamukkale quarry in the East the WNW-ESE-oriented travertine masses are not continuous but are rather distributed in an en-echelon configuration (Fig. 2). This suggests that the underlying blind faults that provide the

necessary fluids for travertine precipitation also have such a configuration. Most faults affecting the subhorizontal to tilted travertine masses are WNW-ESE oriented and are sometimes parallel but mostly slightly obliquely oriented with respect to the incipient margin-bounding faults such as the Düzçalı and Killilk faults, which show a segmented, en-echelon configuration. The paleostress inversion of these en-echelon faults indicates that fault segmentation developed during a long-lived, NNE-SSW oriented extensional-transtensional stress regime (Fig. 12, Fig. 14A-C). The dense and often fault-parallel joint network moreover suggests that faulting was accompanied by fracturing. In the Kömürcüoğlu quarry, for example, joints and faults in the northern part dip steeply to the south whereas joints and faults in the southern part dip moderately to the north. This parallelism would not be present if jointing would post-date faulting.

Due to the shallow burial, tensile Mode I fractures dominate the deformation in the Ballık area. The alignment and consistent orientation of joints and extension veins contribute to the interpretation of the paleostress results as Mode I fractures open perpendicular to minimum principal stress direction ($\sigma_3$), both at shallow (Laubach et al., 2004) or at large depths (Van Noten et al., 2012). As close to the Earth's surface differential stresses are low (Hancock and Engelder, 1989), differences in principal stress magnitudes are small and consequently stress permutations, in which $\sigma_1$, $\sigma_2$ and $\sigma_3$ can shortly swap, may occur. Based on these arguments, Van Noten et al. (2013) concluded that the three dominant joint sets in the Killik dome result from stress permutations in the Pleistocene resulting from NNE-SSW and E-W extension induced by the DGHS Graben and by NW-SE extension from the Baklan Graben (further noted as 'Baklan' extension). Also in the western part of the DGHS, different joint sets observed in fissure ridges reflect multiple extension directions of adjacent basins (Altunel and Hancock, 1993a; Altunel and Karabacak, 2005).

### *6.4 Strike-slip tectonics*

The muddy fault infill and the secondary cementation phases are often striated by subhorizontal slickenlines which are interpreted as strike-slip reactivation features. The strike-slip tectonic stress regime that caused this reactivation clearly post-dates the NNE-SSW extensional phase as strike-slip markers are always observed on normal fault infills and hardly ever as mechanical striations directly on fault walls.

Stress inversion of the Ballık strike-slip fault reactivation data results in an ENE-WSW oriented $\sigma_1$ (compression) and NNW-SSE oriented $\sigma_3$ (extension) (Fig. 12). This orientation is the proper orientation to activate the NNE-SSW Baklan margin faults. The similarity in orientation of $\sigma_3$ during 'Baklan' extension with $\sigma_1$ in the strike-slip regime of the Ballık area strongly suggests that 'Baklan' extension can be interpreted as the reactivation force of the ENE-WSW fault network in the Ballık area. When NW-SE 'Baklan' extension affected the DGHS, the NNE-trending Acıdere fault east of the Ballık area (Figs. 2 and 17) was favourably oriented to be also reactivated as an oblique normal fault (Koçyiğit, 2005) causing subsidence of the Denizli basin floor and uplift of the footwall,

941 i.e. giving rise to the Çökelezdağ Horst (Fig. 14D). To reach this particular stress configuration, $\sigma_2$
942 and $\sigma_3$ in the DGHS switched to change from regional NNE-SSW Denizli extension to regional NW-
943 SE to WNW-ESE 'Baklan' extension.

944 In a fault network, faults tend to involve reactivation of existing faults rather than creating
945 new faults (Scholz, 1998), especially if the fault orientation is in an optimum angle for reactivation
946 (Sibson, 1985). At the time when 'Baklan' extension affected the Acıdere fault, the inherited WNW-
947 ESE Ballık fault network thus acted as border faults for this extension and was, given its favourable
948 orientation, reactivated into sinistral strike-slip faults. The Ballık area can thus be considered as a
949 strike-slip transfer zone from the Acidere fault to the western border fault of the Baklan basin.

950 The Kömürcüoğlu, Gama and Pamukkale travertine masses are preserved from strike-slip
951 faulting. They are situated at the southern end of the Baklan Graben and are thus excluded from the
952 transfer zone and hence neither strike-slip faults or any NE-SW trending joints affected these quarries.
953 Also along the Kepez and Taşkestik Tepe, no strike-slip features are observed as these travertine
954 masses were already uplifted along the margin shoulders and the limited length of the Acidere fault to
955 the north.

956 Another argument of graben interaction was given by Kaymakçı (2006) who modelled the
957 stress magnitudes in the DGHS. He proved that sharp changes occur around subsurface lineaments at
958 places where major basin geometrical changes occur. The change in basin geometry from E to W
959 orientation between Gürleyik and Honaz to a NW to SE orientation between Kocabaş and Ballık (Fig.
960 2) shows that the NW-SE extension of the neighbouring Baklan Graben strongly contributed to the
961 evolution of the eastern DGHS.

962 With exception of the Ballık area, large-scale strike-slip faulting has hardly ever been
963 observed in the DGHS. The only mappable strike-slip faults are two closely-spaced faults affecting
964 the Upper Miocene ancient basin fill in the Alikurt area in the easternmost Kaklık area (see the
965 opposite facing-faults at Alikurt in the eastern part of Fig. 2) (Koçyiğit, 2005) and a NW-trending
966 strike-slip fault at Hierapolis offsetting an historic man-made channel (Altunel and Hancock, 1993b).
967 Kinematic analysis of overprinting slickensides on the former example indicates that a strike-slip
968 regime with ENE-WSW compression has taken place at the end of the Middle Pliocene in the Alikurt
969 area, post-dating an earlier regional NNE-SSW extension phase (Koçyiğit, 2005), quite similar to the
970 tectonic evolution of the Ballık area. This Middle Pliocene phase of strike-slip predates Ballık
971 travertine precipitation but indicates that during the development of the DGHS transient periods of
972 regional stress reconfigurations have taken place at its borders showing tectonic influences of adjacent
973 basins.

974 Similar stress reconfigurations driving fault reactivation are also recognised along the NW
975 margin faults of the Baklan Graben. The Baklan, Acigöl and Burdur halfgrabens are all three bounded
976 by major NW-dipping normal faults and are considered to have initiated parallel to the Dinar transfer
977 zone during the late Miocene-Pliocene in a NW-SE oriented extensional phase (Westaway, 1990).

Further development and NE-SW opening of the Dinar Basin in the Quaternary resulted in sinistral oblique-slip reactivation of the NW-normal faults bounding the Baklan, Acigöl and Burdur Basins, due to differential stretching of the inner blocks on top of the Dinar fault zone (Westaway, 1990; Sintubin et al., 2003; Verhaert et al., 2006; Gürbüz et al., 2012; Alçiçek et al., 2013).

### *6.5 Late Pleistocene – Holocene extension*

During the late Pleistocene – Holocene considerable block tilting has taken place. The NNE-dipping travertine observed in the Reisoğlu-Özaş, Emek, Lower Tuna, Kepez and Taşkestik Tepe and Cinkaya quarries (Figs. 7, 8, 9 and 10) are examples of block tilting as travertine in the hangingwall is tilted northwards towards the footwall as a result of normal faulting. Another example of block tilting occurs in the southern part of the Emek, Kepez and Taşkestik Tepe quarries where travertine in the hangingwall of normal faults dips towards the Denizli Basin to the SSW (Figs. 7C-C' and 11F-F').

Many faults along the northern flank are filled by clayey and marly sediments, either by gravitational of hydrological transport, and calcite cementation along the fault walls is common. The sedimentary infill, open nature of the faults, various fracture patterns and dissolution-enlarged fractures are typical for shallow dilatant fault zones developed along already uplifted extensional graben shoulders (van Ghendt et al., 2010). Fault widening and infill is observed along both strike-slip reactivated and normal faults and can be related to this late deformation stage (Fig. 14E).

The fact that the Killik fault delimits the Killik dome and cuts all faults affecting the Killik dome, suggests that the latest activity in Ballık area took place along the Killik fault. After all, alluvial Quaternary sediments are deposited in the Denizli basin floor in the hangingwall of the Killik fault. The left-lateral stepwise orientation of the Killik fault moreover suggests that a transtensional component was still present in the late-Pleistocene to Holocene causing further oblique opening in this part of the DGHS. Active extension and related travertine precipitation took place further basin inwards illustrated by several travertine ridges at e.g. Kocabaş.

Focal mechanisms of recent earthquakes (Taymaz and Price, 1992; Price and Scott, 1994; Gürbüz et al., 2012; Kaypak and Gökkaya, 2012; Irmak, 2013), geodetic data, southwestwards GPS-based vectors (Elitez and Yaltırak, 2016) and stress indicators on the World Stress Map (e.g. N23E extension for the $M_L$ 4.8 20080425 earthquake at Gürleyik, Fig. 1) all indicate that current extension is still NNE-SSW in the eastern DGHS.

## 7. Conclusions

A detailed structural mapping of neotectonic faults and fractures and a tentative evaluation of the Ballık travertine geodynamic evolution lead to a reconstruction of the kinematic deformation history of the eastern part of the Denizli Graben-Horst System in SW Turkey. This study demonstrates the importance of incorporating tectonic fault analyses into travertine geobody reconstructions to

understand the geodynamic history of continental carbonates. Based on the detailed tectonic analysis and paleostress inversion carried out on fault-slip data gathered from 35 quarries, the following conclusions can be drawn:

1) As one of the best tectonically characterized reservoir-scale travertines, the Ballık travertine forms the ideal base for reservoir modelling with integration of sedimentological and tectonic data from µm to seismic-scale.
2) The Ballık travertine is deformed by WNW-ESE-oriented normal faults that are either parallel or slightly oblique to the Düzçalı and Killik incipient margin-bounding faults. The upper part of the margin was only affected by extension and is marked by backtilted travertine in the hangingwall of normal faults. In the foot- and hangingwall of the Düzçalı fault and in the lower Killik dome, WNW-ESE normal faults are reactivated into sinistral strike-slip faults. Reactivation is evidenced by strike-slip slickenlines that are mostly developed on the muddy fault infill and on polished surfaces of secondary cement infill.
3) Paleostress inversion results in two dominant paleostress regimes. Travertine precipitation and subsequent emplacement of the fault network took place during a long-lived phase of NNE-SSW extension in the early Pleistocene. Block tilting, back rotation, fault infill, secondary fluid flow and extensional fracturing, creating a dense joint network, accompanied faulting during this stress state. The sinistral reactivation of normal faults corresponds to a strike-slip regime with NE-SW to ENE-WSW compression and NW-SE to NNW-SSE extension in the Ballik area. This phase can be related to a NW-SE extensional stress-state during which the NNE-SSW border faults of the Baklan Graben were in extension and during which the edge of the eastern part of the DGHS, i.e. the Acıdere fault, was favourably oriented to be reactivated. The Ballık area acted as a transfer zone in this period. A NNE-SSW extensional phase reinstalled in the late Pleistocene-Holocene causing further fault widening in the Ballık area and active travertine deposition in the central part of the DGHS. This stress state is currently still active.
4) Large travertine deposits are likely to found at graben intersections because of the presence of an underground fault-fracture network that can be formed during different tectonic regimes. Graben intersections are therefore susceptible to an enhanced fluid flow induced by stress permutations and fault reactivation.
5) Based on fault distribution of the Killik dome it is concluded that large domes have a large rigidity with fault development affecting preferentially its flanks but hardly its centre.
6) Faults developed at the intersection of different extensional graben structures can easily reactivate due to stress reconfigurations, whereas this is less common in the middle of such grabens.

## Acknowledgements

The authors would like to thank the numerous quarry owners, workers and engineers in the Ballık area for their kind hospitality, logistic help and interest during field work. This work was undertaken in a collaboration between KU Leuven, Pamukkale University and the Royal Observatory of Belgium during the TraRAS (Joint Industry Project) research project focusing on the architecture of travertine geobodies as reservoir analogue. Marcelle Marques Erthal, Eva De Boever, Jeroen Soete, Michaël Verbiest, Klaus Gessner and an anonymous reviewer are thanked for discussion on the early version of the manuscript. We are grateful to Total, Petrobras and Shell for partial funding.

## Online Supplementary data

**S1:** Google Earth™ Kml-file (cf. Fig. 2) presenting all fault and travertine characteristics discussed in this study. All geomorphological faults surrounding the Ballık area are indicated. Yellow dots indicate the location of the different quarries. Yellow dots are fault observation points. Faults are mapped by connecting individual fault observations. Bedding orientation is indicated by coloured areas and correspond to bedding in Fig. 2: Green areas: S-dipping travertine; Purple: N-dipping travertine; Yellow areas: W-dipping travertine; Brown areas: Marl, sandstone or conglomerate cover deposits; Blue areas: subhorizontal travertine; Blue axis: travertine domal axis..

**S2:** Quarry location information and fault type info. Quarries in the table are organised in same order as they are described in the text. **NF** = normal faulting, **SS** = newly-formed strike-slip faults**, SS r.** = reactivated normal faults with strike-slip kinematics. Non-georeferenced fault and fracture orientation data measured in each quarry is provided for reproducibility. Type (of measurement): Plane (P) orientation noted in dip direction (dd)/dip (d); Lineation (L) noted in in trend (tr) / plunge (pl). A lineation following a plane is the lineation measured on that plane. See kml and Fig. 2 for location of the quarries.

## References

Alçiçek, C., Brogi, A., Capezzuoli, E., Gandin, A., Liotta, D., Meccheri, M., Ruggieri, G., 2015. Extensional structures and hydrothermal fluid flow in Western Anatolia: a review from the Neogene-Quaternary Dinar and Denizli Basins. *Acta Volcanologica* **26(1-2)--27(1-2),** 123-135.

Alçiçek, H., Varol, B., Özkul, M., 2007. Sedimentary facies, depositional environments and palaeogeographic evolution of the Neogene Denizli Basin, SW Anatolia, Turkey. *Sedimentary Geology* **202**(4), 596-637.

Alçiçek, M.C., Brogi, A., Capezzuoli, E., Liotta, D., Meccheri, M., 2013. Superimposed basin formation during Neogene–Quaternary extensional tectonics in SW-Anatolia (Turkey): Insights from the kinematics of the Dinar Fault Zone. *Tectonophysics* **608**, 713-727.

Altunel, E., 1994. Active tectonics and the evolution of Quaternary travertines at Pamukkale, Western Turkey. PhD thesis, University of Bristol, pp 236.

Altunel, E., 2000. Historical earthquake activity in and around Hierapolis. In: D'Andria, F., Silvestrelli, F. (Eds.), Ricerche Archeologiche Turche Nella Valle Del Lykos, Lykos Vadisi Turk Arkeoloji Arastirmalari. Congedo Editore. (in Italian and Turkish). p. 299-325

Altunel, E., Hancock, P.L., 1993a. Active fissuring and faulting in Quaternary travertines at Pamukkale, western Turkey. *Z Geomorph NF* **94**, 285 - 302.

1091 Altunel, E., Hancock, P.L., 1993b. Morphology and structural setting of Quaternary travertines at Pamukkale,
1092 western Turkey. *Geological Journal* **28**, 335-346.
1093 Altunel, E., Hancock, P.L., 1996. Structural Attributes of Travertine-Filled Extensional Fissures in the
1094 Pamukkale Plateau, Western Turkey. *International Geology Review* **38**(8), 768-777.
1095 Altunel, E., Karabacak, V., 2005. Determination of horizontal extension from fissure-ridge travertines: a case
1096 study from the Denizli Basin, southwestern Turkey. *Geodinamica Acta* **18**(3-4), 333-342.
1097 Angelier, J., Mechler, P., 1977. Sur une méthode graphique de recherche des contraintes principales également
1098 utilisable en tectonique et en séismologie: la méthode des dièdres droits. *Bulletin de la Société géologique de*
1099 *France* **(7)19**(6), 1309-1318.
1100 Bott, M.P.H., 1959. The mechanics of oblique-slip faulting. *Geological Magazine* **96**, 109–117.
1101 Bozkurt, E., 2001. Neotectonics of Turkey - a synthesis. *Geodinamica Acta* **14**, 3-30.
1102 Bozkurt, E., Sözbilir, H., 2006. Evolution of the Large-scale Active Manisa Fault, Southwest Turkey:
1103 Implications on Fault Development and Regional Tectonics. *Geodinamica Acta* **19**(6), 427-453.
1104 Brogi, A., 2004. Faults linkage, damage rocks and hydrothermal fluid circulation: Tectonic interpretation of the
1105 Rapolano Terme travertines (southern Tuscany, Italy) in the context of Northern Apennines Neogene–
1106 Quaternary extension. *Eclogae geol. Helv.* **97**, 307-320.
1107 Brogi, A., Capezzuoli, E., 2009. Travertine deposition and faulting: the fault-related travertine fissure-ridge at
1108 Terme S. Giovanni, Rapolano Terme (Italy). *International Journal of Earth Sciences* **98**, 931-947.
1109 Brogi, A., Capezzuoli, E., 2014. Earthquake impact on fissure-ridge type travertine deposition. *Geological*
1110 *Magazine. Rapid Communication*, 1-9.
1111 Brogi, A., Capezzuoli, E., Alçiçek, M.C., Gandin, A., 2014. Evolution of a fault-controlled fissure-ridge type
1112 travertine deposit in the western Anatolia extensional province: the Çukurbağ fissure-ridge (Pamukkale,
1113 Turkey). *Journal of the Geological Society*.
1114 Brogi, A., Capezzuoli, E., Aqué, R., Branca, M., Voltarrio, M., 2010. Studying travertine for neotectonic
1115 investigations: Middle-Late Pleistocene syn-tectonic travertine deposition at Serra di Rapolano (Northern
1116 Apennines, Italy). *International Journal of Earth Sciences* **99**, 1383-1398.
1117 Brogi, A., Capezzuoli, E., Buracchi, E., Branca, M., 2012. Tectonic control on travertine and calcareous tufa
1118 deposition in a low-temperature geothermal system (Sarteano, Central Italy). *Journal of the Geological*
1119 *Society* **169**(4), 461-476.
1120 Buckley, J.P., Elders, C., Mann, J., 2013. Carbonate Buildups in the Santos Basin, Offshore Brazil. *Programme*
1121 *and Abstract Volume: Microbial Carbonates in Space and Time: Implications for Global Exploration and*
1122 *Production. The Geological Society. 19−20 June, 2013.*
1123 Çakır, Z., 1999. Along-strike discontinuities of active normal faults and its influence on Quaternary travertine
1124 deposition; examples from western Turkey, Turkish Journal of Earth Sciences, 8, 67-80. *Turkish Journal of*
1125 *Earth Sciences* **8**, 67-80.
1126 Capezzuoli, E., Gandin, A., Sandrelli, F., 2010. Calcareous tufa as indicators of climatic variability: a case study
1127 from southern Tuscany (Italy). *Geological Society, London, Special Publications* **336**(1), 263-281.
1128 Çelik, S., Çobanoğlu, İ., Atatanır, L., 2014. General material properties of Denizli (SW Turkey) travertines as a
1129 building stone. *Bulletin of Engineering Geology and the Environment* **73**(3), 825-838.
1130 Çiftçi, N.B., Bozkurt, E., 2009. Pattern of normal faulting in the Gediz Graben, SW Turkey. *Tectonophysics*
1131 **473**(1–2), 234-260.
1132 Claes, H., Degros, M., Soete, J., Claes, S., Kele, S., Mindszenty, A., Török, Á., El Desouky, H., Vanhaecke, F.,
1133 Swennen, R., 2017a. Geobody architecture, genesis and petrophysical characteristics of the Budakalász
1134 travertines, Buda Hills (Hungary). *Quaternary International* **437**, 107-128.
1135 Claes, H., Erthal, M., Soete, J., Özkul, M., Swennen, R., 2017b. Shrub and pore type classification: Petrography
1136 of travertine shrubs from the Ballık-Belevi area (Denizli, SW Turkey). *Quaternary International* **437**, 147–
1137 163.
1138 Claes, H., Soete, J., Van Noten, K., El Desouky, H., Marques Erthal, M., Vanhaecke, F., Özkul, M., Swennen,
1139 R., 2015. Sedimentology, three-dimensional geobody reconstruction and carbon dioxide origin of
1140 Pleistocene travertine deposits in the Ballık area (south-west Turkey). *Sedimentology* **62**, 1408-1445.
1141 Çobanoğlu, I., Çelik, S.B., 2012. Determination of strength parameters and quality assessment of Denizli
1142 travertines (SW Turkey). *Engineering Geology* **129-130**, 38-47.
1143 Çolak Erol, S., Özkul, M., Aksoy, E., Kele, S., Ghaleb, B., 2015. Travertine occurrences along major strike-slip
1144 fault zones: Structural, depositional and geochemical constraints from the Eastern Anatolian fault System
1145 (EAFS), Turkey. *Geodinamica Acta, DOI: 10.1080/09853111.2014.979530*.
1146 De Boever, E., Foubert, A., Lopez, B., Swennen, R., Jaworowski, C., Özkul, M., Virgone, A., 2017.
1147 Comparative study of the Pleistocene Cakmak quarry (Denizli Basin,Turkey) and modern Mammoth Hot
1148 Springs deposits (Yellowstone National Park, USA). *Quaternary International* **437**, 129-146.

De Boever, E., Foubert, A., Oligschlaeger, D., Claes, S., Soete, J., Bertier, P., Özkul, M., Virgone, A., Swennen, R., 2016. Multiscale approach to (micro)porosity quantification in continental spring carbonate facies: Case study from the Cakmak quarry (Denizli, Turkey). *Geochemistry, Geophysics, Geosystems* **17**(7), 2922-2939.

De Filippis, L., Billi, A., 2012. Morphotectonics of fissure ridge travertines from geothermal areas of Mammoth Hot Springs (Wyoming) and Bridgeport (California). *Tectonophysics* **548-549**, 34-48.

De Filippis, L., Faccenna, C., Billi, A., Anzalone, E., Brilli, M., Özkul, M., Soligo, M., Tuccimei, P., Villa, I.M., 2012. Growth of fissure ridge travertines from geothermal springs of Denizli Basin, western Turkey. *Geological Society of America Bulletin* **124**, 1629-1645.

De Filippis, L., Faccenna, C., Billi, A., Anzalone, E., Brilli, M., Soligo, M., Tuccimei, P., 2013. Plateau versus fissure ridge travertines from Quaternary geothermal springs of Italy and Turkey: Interactions and feedbacks between fluid discharge, paleoclimate, and tectonics. *Earth-Science Reviews* **123**(0), 35-52.

Delvaux, D., Sperner, B., 2003. Stress tensor inversion from fault kinematic indicators and focal mechanism data: the TENSOR program. In: Nieuwland, D. (Eds.), New Insights into Structural Interpretation and Modelling. Geological Society, London, Special Publications, 212: 75-100.

El Desouky, H., Soete, J., Claes, H., Özkul, M., Vanhaecke, F., Swennen, R., 2015. Novel applications of fluid inclusions and isotope geochemistry in unravelling the genesis of fossil travertine systems. *Sedimentology* **62**(1), 27-56.

Elitez, İ., Yaltırak, C., 2016. Miocene to Quaternary tectonostratigraphic evolution of the middle section of the Burdur-Fethiye Shear Zone, south-western Turkey: Implications for the wide inter-plate shear zones. *Tectonophysics* **690**, 336-354.

Faccenna, C., 1994. Structural and hydrogeological features of Pleistocene shear zones in the area of Rome (Central Italy). *Annali di Geoficia* **37**(1), 121-133.

Faccenna, C., Soligo, M., Billi, A., De Filippis, L., Funiciello, R., Rossetti, C., Tuccimei, P., 2008. Late Pleistocene depositional cycles of the Lapis Tiburtinus travertine (Tivoli, Central Italy): Possible influence of climate and fault activity. *Global and Planetary Change* **63**(4), 299-308.

Gessner, K., Gallardo, L.A., Markwitz, V., Ring, U., Thomson, S.N., 2013. What caused the denudation of the Menderes Massif: Review of crustal evolution, lithosphere structure, and dynamic topography in southwest Turkey. *Gondwana Research* **24**(1), 243-274.

González-Martín, J.A., García del Cura, M.A., Ordóñez, S., 1989. Formaciones tobaceas en los valles Tajuña y Tajo. In: *Excursion Guide C-4. Reunion del Cuaternario Iberico, Madrid 25–29 September 1989. Association of Española Estudio del Cuaternario (AEQUA) – Grupo Trabalho Portugies Estudodo Quaternario (GTPEQ).*

Guo, L., Riding, R., 1998. Hot-spring travertine facies and sequences, Late Pleistocene, Rapolano Terme, Italy. *Sedimentology* **45**, 163-180.

Gürbüz, A., Boyraz, S., Ismael, M.T., 2012. Plio-Quaternary development of the Baklan–Dinar graben: implications for cross-graben formation in SW Turkey. *International Geology Review* **54**(1), 33-50.

Hancock, P.L., Chalmers, R.M.L., Altunel, E., Çakir, Z., 1999. Travitonics: using travertines in active fault studies. *Journal of Structural Geology* **21**, 903-916.

Hancock, P.L., Engelder, T., 1989. Neotectonic joints. *Geological Society of America Bulletin* **101**(10), 1197-1208.

Irmak, S., 2013. Focal mechanisms of small-moderate earthquakes in Denizli Graben (SW Turkey). *Earth Planets Space* **65**, 943-955.

Irmak, S., Taymaz, T., 2009. Source Mechanics of Recent Moderate Earthquakes Occurred in Honaz-Denizli (W Turkey) Graben Obtained by Regional Broadband Waveform Inversion. In: *International Symposium on Historical Earthquakes and Conservation of Monuments in the Eastern Mediterranean Region*, Istanbul, Turkey, 350-356.

Kaymakçı, N., 2006. Kinematic development and paleostress analysis of Denizli Basin (W Turkey): implications of spatial variation of relative paleostress magnitudes and orientations. *Journal of Asian Earth Sciences* **27**, 207-222.

Kaypak, B., Gökkaya, G., 2012. 3-D imaging of the upper crust beneath the Denizli geothermal region by local earthquake tomography, western Turkey. *Journal of Volcanology and Geothermal Research* **211-212**, 47–60.

Kele, S., Demény, A., Siklósy, Z., Németh, T., Tóth, M., Kovács, M.B., 2008. Chemical and stable isotope composition of recent hot-water travertines and associated thermal waters, from Egerszalók, Hungary: Depositional facies and non-equilibrium fractionation. *Sedimentary Geology* **211**(3–4), 53-72.

Kele, S., Özkul, M., Fórizs, I., Gökgöz, A., Baykara, M.O., Alçiçek, M.C., Németh, T., 2011. Stable isotope geochemical study of Pamukkale travertines: New evidences of low-temperature non-equilibrium calcite-water fractionation. *Sedimentary Geology* **238**(1–2), 191-212.

Khatib, S., Rochette, P., Alçiçek, M.C., Lebatard, A.-E., Demory, F., Saos, T., 2014. Études stratigraphique, sédimentologique et paléomagnétique des travertins de Kocabaş, Bassin de Denizli, Anatolie, Turquie, contenant des restes fossiles quaternaires. *L'Anthropologie* **118**(1), 16-33.

Kipata, M.L., Delvaux, D., Sebagenzi, M.N., Cailteux, J., Sintubin, M., 2013. Brittle tectonic and stress field evolution in the Pan-African Lufilian arc and its foreland (Katanga, DRC): from orogenic compression to extensional collapse, transpressional inversion and transition to rifting. *Geologica Belgica* **16**(1-2), 1-17.

Koçyiğit, A., 2005. The Denizli graben-horst system and the eastern limit of western Anatolian continental extension: basin fill, structure, deformational mode, throw amount and episodic evolutionary history, SW Turkey. *Geodinamica Acta* **18**(3-4), 167-208.

Laubach, S.E., Olson, J.E., Gale, J.F.W., 2004. Are open fractures necessarily aligned with maximum horizontal stresses? *Earth and Planetary Science Letters* **222**, 191-195.

Lebatard, A.-E., Alçiçek, M.C., Rochette, P., Khatib, S., Vialet, A., Boulbes, N., Bourlès, D.L., Demory, F., Guipert, G., Mayda, S., Titov, V.V., Vidal, L., de Lumley, H., 2014. Dating the Homo erectus bearing travertine from Kocabaş (Denizli, Turkey) at at least 1.1 Ma. *Earth and Planetary Science Letters* **390**, 8-18.

Loveless, S., Bense, V., Turner, J., 2011. Fault architecture and deformation processes within poorly lithified rift sediments, Central Greece. *Journal of Structural Geology* **33**(11), 1554-1568.

Maggi, M., Cianfarr, P., Salvini, F., Coelho de Lima, C., 2015. Staircase fractures in microbialites and the role of lamination-related mechanical anisotropy: The example of the Acquasanta Terme travertine deposits (central Italy). *GSA bulletin* **127**, 879-896.

Martínez-Díaz, J.J., Hernández-Enrile, J.L., 2001. Using travertine deformations to characterize paleoseismic activity along an active oblique-slip fault: the Alhama de Murcia fault (Betic Cordillera, Spain). *Geologica Acta* **36**(3-4), 297-313.

McKenzie, D., 1970. The plate tectonics of the Mediterranean region. *Nature* **226**, 239-243.

Mesci, B.L., Gursoy, H., Tatar, O., 2008. The Evolution of Travertine Masses in the Sivas Area (Central Turkey) and Their Relationships to Active Tectonics. *Turkish Journal of Earth Sciences* **17**, 219-240.

Nemec, W., Steel, R.J., 1984. Alluvial and Coastal Conglomerates: Their Significant Features and Some Comments on Gravelly Mass-Flow Deposits. *Sedimentology of Gravels and Conglomerates* **10**, 1-31.

Özkaymak, Ç., 2015. Tectonic analysis of the Honaz Fault (western Anatolia) using geomorphic indices and the regional implications. *Geodinamica Acta* **27**(2-3), 110-129.

Özkul, M., Engin, B., Alçiçek, M.C., Koralay, T., Demirtaş, H., 2004. Thermoluminescence dating of Quaternary hot spring travertines and some implications on graben evolution, Denizli, Western Turkey. In: *32nd International Geological Congress, August 20–28, 2004, Florence, Italy*.

Özkul, M., Gökgöz, A., HorvatinčIć, N., 2010. Depositional properties and geochemistry of Holocene perched springline tufa deposits and associated spring waters: a case study from the Denizli Province, Western Turkey. *Geological Society, London, Special Publications* **336**(1), 245-262.

Özkul, M., Gökgöz, A., Kele, S., Baykara, M.O., Shen, C.-C., Chang, Y.-W., Kaya, A., Hançer, M., Aratman, C., Akin, T., Örü, Z., 2014. Sedimentological and geochemical characteristics of a fluvial travertine: A case from the eastern Mediterranean region. *Sedimentology* **61**(1), 291-318.

Özkul, M., Kele, S., Gökgöz, A., Shen, C.-C., Jones, B., Baykara, M.O., Fórizs, I., Németh, T., Chang, Y.-W., Alçiçek, M.C., 2013. Comparison of the quaternary travertine sites in the Denizli extensional basin based on their depositional and geochemical data. *Sedimentary Geology*.

Özkul, M., Varol, B., Alçiçek, M.C., 2002. Depositional environments and petrography of the Denízlí travertines. *Miner. Res. Expl. Bull.* **125**, 13-29.

Piccardi, L., 2007. The ad 60 Denizli Basin earthquake and the apparition of Archangel Michael at Colossae (Aegean Turkey). *Geological Society, London, Special Publications* **273**(1), 95.

Price, S.P., Scott, B., 1994. Fault-block rotations at the edge of a zone of continental extension; southwest Turkey. *Journal of Structural Geology* **16**(3), 381-392.

Reading, H.G., 1996. *Sedimentary Environments; Processes, Facies and Stratigraphy*. London, Blackwell Science, 688 p.

Röller, K., Trepmann, C.A., 2003. Stereo32 version 1.0.2. Ruhr Universität Bohum.

Saller, A., Rushton, S., Buambua, L., Inman, K., McNeil, R. Dickson, J.A.D. 2016. Presalt stratigraphy and depositional systems in the Kwanza Basin, offshore Angola. AAPG Bulletin, 100, 1135–1164.

Scholz, C.H., 1998. Earthquakes and friction laws. *Nature* **391**(37-42).

Seyítoğlu, G., Scott, B.C., 1996. The cause of N-S extensional tectonics in western Turkey: Tectonic escape vs back-arc spreading vs orogenic collapse. *Journal of Geodynamics* **22**(1), 145-153.

Sharp, I., Verwer, K., Ferreira, H., Lapponi, F., Snidero, M., Machado, V., Holtar, E., Swart, R., Marsh, J., Gindre, L., Puigdefabregas, C., Fejerskov, M., 2013. Pre- and Post-Salt Non-Marine Carbonates of the Namibe Basin, Angola. *Programme and Abstract Volume: Microbial Carbonates in Space and Time: Implications for Global Exploration and Production. The Geological Society. 19-20 June, 2013*.

Sibson, R., 1985. A note on fault reactivation. *Journal of Structural Geology* **7**(6), 751-754.

Sintubin, M., Muchez, P., Similox-Tohon, D., Verhaert, G., Paulissen, E., Waelkens, M., 2003. Seismic catastrophes at the ancient city of Sagalassos (SW Turkey) and their implications for seismotectonics in the Burdur–Isparta area. *Geological Journal* **38**(3-4), 359-374.

Soete, J., Kleipool, L.M., Claes, H., Claes, S., Hamaekers, H., Kele, S., Özkul, M., Foubert, A., Reijmer, J.J.G., Swennen, R., 2015. Acoustic properties in travertines and their relation to porosity and pore types. *Marine and Petroleum Geology* **59**, 320-335.

Taymaz, T., Price, S., 1992. The 1971 May 12 Burdur Earthquake sequence, SW Turkey - a synthesis of seismological and geological observations. *Geophysical Journal International* **108**, 589–603.

Temiz, U., Gökten, Y.E., Eikenberg, J., 2013. Strike-slip deformation and U/Th dating of travertine deposition: Examples from North Anatolian Fault Zone, Bolu and Yeniçağ Basins, Turkey. *Quaternary International* **312**(0), 132-140.

ten Veen, J.H., Boulton, S.J., Alçiçek, M.C., 2009. From palaeotectonics to neotectonics in the Neotethys realm: The importance of kinematic decoupling and inherited structural grain in SW Anatolia (Turkey). *Tectonophysics* **473**(1–2), 261-281.

Toker, E., Kayseri-Özer, M.S., Özkul, M., Kele, S., 2014. Depositional system and palaeoclimatic interpretations of Middle to Late Pleistocene travertines: Kocabaş, Denizli, south-west Turkey. *Sedimentology* **62**, 1360-1383.

Topal, S., 2012. Denizli havzasındaki fayların tektonik jeomorfolojisi. Unpublished PhD thesis Pamukkale University, 145 p. (in Turkish with English abstract). Unpublished PhD thesis.

Topal, S., Özkul, M., 2014. Soft-Sediment Deformation Structures Interpreted as Seismites in the Kolankaya Formation, Denizli Basin (SW Turkey). *The Scientific World Journal. Article ID 352654*, 13 p.

van Ghendt, H.W., Holland, M., Urai, J.L., Loosveld, R., 2010. Evolution of fault zones in carbonates with mechanical stratigraphy - Insights from scale models using layered cohesive powder. *Journal of Structural Geology* **32**, 1375-1391.

van Hinsbergen, D.J.J., Kaymakci, N., Spakman, W., Torsvik, T.H., 2010. Reconciling the geological history of western Turkey with plate circuits and mantle tomography. *Earth and Planetary Science Letters* **297**(3-4), 674-686.

Van Noten, K., Soete, J., Claes, H., Foubert, A., Özkul, M., Swennen, R., 2013. Fracture networks and strike-slip deformation along reactivated normal faults in Quaternary travertine deposits, Denizli Basin, Western Turkey. *Tectonophysics* **588**, 154-170.

Van Noten, K., Van Baelen, H., Sintubin, M., 2012. The complexity of 3D stress-state changes during compressional tectonic inversion at the onset of orogeny. In: Healy, D., Butler, R.W.H., Shipton, Z.K., Sibson, R.H. (Eds.), Faulting, Fracturing, and Igneous Intrusion in the Earth's crust. Geological Society, London, Special Publications 367, 51-69.

Verhaert, G., Similox-Tohon, D., Vandycke, S., Sintubin, M., Muchez, P., 2006. Different stress states in the Burdur-Isparta region (SW Turkey) since Late Miocene times: a reflection of a transient stress regime. *Journal of Structural Geology* **28**, 1067–1083.

Wallace, R.E., 1951. Geometry of shearing stress and relation to faulting. *Journal of Geology* **69**, 118–130.

Wang, Z., Meyer, M.C., Gliganic, L.A., Hoffmann, D.L., May, J.-H., 2017. Timing of fluvial terrace formation and concomitant travertine deposition in the upper Sutlej River (Tirthapuri, southwestern Tibet) and paleoclimatic implications. *Quaternary Science Reviews* **169**, 357-377.

Westaway, R., 1990. Block rotation in western Turkey, 1. Observational evidence. *J. of Geo. Res.* **95**, 19857-19884.

Westaway, R., 1993. Neogene evolution of the Denizli region of western Turkey. *Journal of Structural Geology* **15**, 37-53.

Westaway, R., Guillou, H., Yurtmen, S., Demir, T., Scaillet, S., Rowbotham, G., 2005. Constraints on the timing and regional conditions at the start of the present phase of crustal extension in western Turkey, from observations in and around the Denizli region. *Geodinamica Acta* **18**(3-4), 209-238.

Westaway, R., Pringle, M., Yurtmen, S., Demir, T., Bridgland, D., Rowbotham, G., Maddy, D., 2003. Pliocene and Quaternary surface uplift of western Turkey revealed by long-term river terrace sequences. *Current Science* **84**(8), 1090-1101.

Yalçiner, C.C., 2013. Investigation of the subsurface geometry of fissure-ridge travertine with GPR, Pamukkale, western Turkey. *J. Geophys. Eng.* **10. 035001**, 10pp.